

Unitary Isobar Model - MAID2007

D. Drechsel¹, S. S. Kamalov², L. Tiator¹

¹ Institut für Kernphysik, Universität Mainz, D-55099 Mainz

² JINR Dubna, 141980 Moscow Region, Russia

October 1, 2007

Abstract. The unitary isobar model MAID2007 has been developed to analyze the world data of pion photo- and electroproduction. The model contains both a common background and several resonance terms. The background is unitarized according to the K-matrix prescription, and the 13 four-star resonances with masses below 2 GeV are described by appropriately unitarized Breit-Wigner forms. The data have been analyzed by both single-energy and global fits, and the transverse and longitudinal helicity amplitudes have been extracted for the four-star resonances below 2 GeV. Because of its inherent simplicity, MAID2007 is well adopted for predictions and analysis of the observables in pion photo- and electroproduction.

PACS. 11.80.Et , 13.40.-f, 13.60.Le, 14.20.Gk

1 Introduction

Our knowledge about the excitation spectrum of the nucleon was originally provided by elastic pion-nucleon scattering [1]. All the resonances listed in the Particle Data Tables [2] have been identified by partial-wave analyses of this process with both Breit-Wigner and pole extraction techniques. From such analyses we know the resonance masses, widths, and branching ratios into the πN and $\pi\pi N$ channels. These are reliable parameters for the resonances in the 3- and 4-star tiers, with only few exceptions. In particular, there remains some doubt about the structure of two prominent resonances, the Roper $P_{11}(1440)$, which appears unusually broad, and the $S_{11}(1535)$, where the pole can not be uniquely determined, because it lies close to the ηN threshold.

On the basis of these relatively firm grounds, additional information can be obtained for the electromagnetic (e.m.) γNN^* couplings through pion photo- and electroproduction. These couplings are described by electric, magnetic, and charge transition form factors, $G_E^*(Q^2)$, $G_M^*(Q^2)$, and $G_C^*(Q^2)$, or by linear combinations thereof as helicity amplitudes $A_{1/2}(Q^2)$, $A_{3/2}(Q^2)$, and $S_{1/2}(Q^2)$. So far we have some reasonable knowledge of the transverse amplitudes $A_{1/2}$ and $A_{3/2}$ at the real photon point, which are tabulated in the Particle Data Tables. For finite Q^2 the information found in the literature is scarce and until recently practically nonexistent for the longitudinal amplitudes $S_{1/2}$. But even for the transverse amplitudes only few results have remained firm over the recent years, such as the G_M^* form factor of the $P_{33}(1232)$ or $\Delta(1232)$ resonance up to $Q^2 \approx 10 \text{ GeV}^2$, the $A_{1/2}(Q^2)$ for the $S_{11}(1535)$ up to $Q^2 \approx 5 \text{ GeV}^2$, and the helicity

asymmetry $\mathcal{A}(Q^2)$ for the resonances $D_{13}(1520)$ and $F_{15}(1680)$ up to $Q^2 \approx 3 \text{ GeV}^2$ [3]. Frequently also data points for other resonances, e.g., the Roper resonance, are shown together with quark model calculations. However, the statistical errors are often quite large and the model dependence of the analysis may be even larger. In this context it is worth mentioning that also the notion of a ‘data point’ is somewhat misleading because the photon couplings and amplitudes can only be derived indirectly by a partial-wave analysis. It is in fact prerequisite to analyze a particular experiment within a framework based on the “world data”. The only exception from this caveat is the $\Delta(1232)$ resonance. For this lowest-lying and strongest resonance of the nucleon, the analysis is facilitated by two important constraints: the validity of (I) the Watson theorem at the 1 % level and (II) the truncation of the multipole series to S and P waves as a good first-order approximation. With these assumptions the e.m. couplings have been directly determined in the real photon limit by a complete experiment with polarized photons and detecting both neutral and charged pions in the final state, thus allowing also for an isospin separation [4]. Moreover, a nearly complete separation of the possible polarization observables has recently provided the basis to extend such a “model-independent” analysis also to electroproduction [5]. However, we are still far from such a situation for all the higher resonances. Neither are the mentioned constraints valid nor are we close to a complete experiment. Until recently the data base was rather limited, the error bars were large, and no data were available from target or recoil polarization experiments. Even now there exist only very few data points from double-polarization experiments at energies above the $\Delta(1232)$. However, the situation for

unpolarized $e + p \rightarrow e' + p + \pi^0$ reaction has considerably improved, mainly by new JLab experiments in all three halls A, B, and C. These data cover a large energy range from the $\Delta(1232)$ up to the third resonance region with a wide angular range in θ_π . Furthermore, electron beam polarization has been used in several experiments at JLab, MIT/Bates, and MAMI/Mainz. Because of the large coverage in the azimuthal angle by the modern large-acceptance detectors, a separation of all 4 partial cross sections in the unpolarized experiment becomes possible. But even without a Rosenbluth separation of the transverse (σ_T) and longitudinal (σ_L) cross sections, there is an enhanced sensitivity to the longitudinal amplitudes due to the interference terms σ_{LT} and $\sigma_{LT'}$. Such data are the basis of our new partial-wave analysis with an improved version of the Mainz unitary isobar model MAID.

We proceed by presenting a brief history of the unitary isobar model in Sect. 2. The formalism of pion photo- and electroproduction is summarized in Sect. 3. In the following Sect. 4 we present our results for photoproduction as obtained from the latest version MAID2007, and in Sect. 5 this analysis is extended to electroproduction. We conclude with a short summary in Sect. 6.

2 History of MAID

– MAID98

In 1998 the first version of the Unitary Isobar Model was developed and implemented on the web to give an easy access for the community. MAID98 was constructed with a limited set of nucleon resonances described by Breit-Wigner forms and a non-resonant background constructed from Born terms and t-channel vector-meson contributions [6]. In order to have the right threshold behavior and a reasonable description at the higher energies, the Born terms were introduced with an energy-dependent mixing of pseudovector and pseudoscalar πNN coupling. Each partial wave was unitarized up to the two-pion threshold by use of Watson's theorem. Specifically, the unitarization was achieved by introducing additional phases ϕ_R in the resonance amplitudes in order to adjust the phase of the total amplitude. Only the following 4-star resonances were included: $P_{33}(1232)$, $P_{11}(1440)$, $D_{13}(1520)$, $S_{11}(1535)$, $S_{11}(1650)$, $F_{15}(1680)$, and $D_{33}(1700)$. The e.m. vertices of these resonances were extracted from a best fit to the VPI/GWU partial-wave analysis [7]. For the $P_{33}(1232)$ resonance, we determined the following ratios of transition amplitudes: (I) electric quadrupole to magnetic dipole transition, $R_{EM} = E2/M1 = -2.2\%$, and (II) electric Coulomb to magnetic dipole transition, $R_{CM} = C2/M1 = -3.6\%$, independent of the 4-momentum transfer Q^2 . The Q^2 -dependence of the resonance amplitudes in the second and third resonance regions was expressed in terms of the quark electric

and magnetic multipoles [8]. The non-unitarized background contributions were determined using standard Born terms and vector-meson exchange. In order to preserve gauge invariance, the Born terms were expressed by the usual dipole form for the Sachs form factors, and both the pion and the axial form factor were set equal to the isovector Dirac form factor, $F_\pi(Q^2) = G_A(Q^2) = F_1^p(Q^2) - F_1^n(Q^2)$.

– MAID2000

In this version of MAID, the background contribution was unitarized for the multipoles up to F waves according to the prescription of K-matrix theory. The S -wave multipoles E_{0+} and L_{0+} were modified in order to improve their energy dependence in the threshold region. With the new unitarization procedure, the pion photoproduction multipoles of SAID and some selected data for pion photo- and electroproduction in the energy range up to $W = 1.6$ GeV were fitted [9]. The ratios of the $\Delta(1232)$ multipoles were found to be $R_{EM} = -2.2\%$ and $R_{CM} = -6.5\%$, still independent of Q^2 .

– MAID2003

In accordance with results of Ref. [10], the Q^2 dependence of the electric and Coulomb excitations of the $\Delta(1232)$ resonance was modified. The ratio R_{EM} was found to change sign at $Q^2 \approx 3.3$ GeV² from negative to positive values, and R_{CM} decreased from -6.5% at $Q^2 = 0$ to -13.5% at $Q^2 = 4$ GeV². Moreover, the following 4-star resonances were included in MAID2003: $S_{31}(1620)$, $D_{15}(1675)$, $P_{13}(1720)$, $F_{35}(1905)$, $P_{31}(1910)$, and $F_{37}(1950)$. In contrast to previous versions, the helicity amplitudes of all 13 resonances were input parameters and their Q^2 dependence was parameterized by polynomials. With this new version of MAID we directly analyzed all the pion photo- and electroproduction data available since 1960, and for the first time we made local (single energy) and global (energy dependent) fits, independent of the GWU/SAID group.

– MAID2005

The Q^2 dependence of the Sachs form factors in the Born terms was replaced by the more recent parameterization of Ref. [11], and at the e.m. vertices of the pion-pole and seagull terms, realistic pion and axial form factors were introduced. As a result the description of charged pion electroproduction was much improved. On the basis of a large amount of new data from MIT/Bates, ELSA/Bonn, Grenoble, Mainz, and Jefferson Lab, we performed new local and global as well as single- Q^2 fits and obtained a better description of the data in the energy range 1.6 GeV $< W < 2$ GeV [12].

– MAID2007

The present version of MAID is presented in some detail in the following sections. As far as pion photoproduction is concerned, this version is identical to MAID2005. The main changes are related to the Q^2 evolution of e.m. form factors. In particular, the Q^2 -dependence of the $\Delta(1232)$ transition form factors are

remodeled to be consistent with the Siegert theorem. As a result the ratio R_{CM} decreases sharply if Q^2 approaches zero. Furthermore, our analysis of the recent high- Q^2 data [13] led to the conclusion that R_{EM} remains negative in the range of the existing experiments.

3 Formalism for pion photo- and electroproduction

Let us first define the kinematics of pion photo- and electroproduction on a nucleon,

$$\gamma^*(k) + N(p) \rightarrow \pi(q) + N'(p'), \quad (1)$$

where the variables in brackets denote the 4-momenta of the participating particles. In the pion-nucleon center-of mass (c.m.) system, we define

$$k^\mu = (\omega_\gamma, \mathbf{k}), \quad q^\mu = (\omega_\pi, \mathbf{q}), \quad p^\mu = (E_N, -\mathbf{k}), \quad (2)$$

where

$$k(W, Q^2) = |\mathbf{k}| = \sqrt{\left(\frac{W^2 - m^2 - Q^2}{2W}\right)^2 + Q^2}, \quad (3)$$

$$q(W) = |\mathbf{q}| = \sqrt{\left(\frac{W^2 - m^2 + m_\pi^2}{2W}\right)^2 - m_\pi^2}, \quad (4)$$

with $W = \omega_\gamma + E_N$ the total c.m. energy and $Q^2 = k^2 - \omega_\gamma^2 > 0$ the square of 4-momentum deposited by the photon at the nucleon vertex, also referred to as the virtuality of the photon. In order to simplify the notation, we use the following abbreviations:

$$k_W = k(W, 0) = \frac{W^2 - m^2}{2W}, \quad (5)$$

describing the momentum of a real photon, and

$$k_R = k(M_R, 0), \quad q_R = q(M_R), \quad (6)$$

for the real photon and pion momenta at the resonance position, $W = M_R$.

The basic equations used for MAID2007 are taken from the dynamical Dubna-Mainz-Taipei (DMT) model [10, 14, 15]. In this approach the t-matrix for pion photo- and electroproduction takes the form

$$t_{\gamma\pi}(W) = v_{\gamma\pi}(W) + v_{\gamma\pi}(W) g_0(W) t_{\pi N}(W), \quad (7)$$

with $v_{\gamma\pi}$ the transition potential for the reaction $\gamma^* N \rightarrow \pi N$, $t_{\pi N}$ the πN scattering matrix, and g_0 the free πN propagator. In a resonant channel the transition potential $v_{\gamma\pi}$ consists of two terms,

$$v_{\gamma\pi}(W) = v_{\gamma\pi}^B(W) + v_{\gamma\pi}^R(W), \quad (8)$$

with $v_{\gamma\pi}^B$ the background transition potential and $v_{\gamma\pi}^R$ the contribution of the “bare” resonance excitation. The resulting t-matrix can be decomposed into two terms [15]

$$t_{\gamma\pi}(W) = t_{\gamma\pi}^B(W) + t_{\gamma\pi}^R(W), \quad (9)$$

where

$$t_{\gamma\pi}^B(W) = v_{\gamma\pi}^B(W) + v_{\gamma\pi}^B(W) g_0(W) t_{\pi N}(W), \quad (10)$$

$$t_{\gamma\pi}^R(W) = v_{\gamma\pi}^R(W) + v_{\gamma\pi}^R(W) g_0(W) t_{\pi N}(W), \quad (11)$$

with $t_{\gamma\pi}^B$ including the contributions from both the non-resonant background and the $\gamma^* N R$ vertex renormalization. The decomposition in resonance and background contributions is not unique, however, our definition has the advantage that all the processes starting with the e.m. excitation of a bare resonance are summed up in $t_{\gamma\pi}^R$.

3.1 Unitarized background

The multipole decomposition of Eq. (10) yields the background contribution to the physical amplitudes in the channels $\alpha = (\xi, \ell, j, I)$ [14], where ℓ , j and I denote the orbital momentum, the total angular momentum, and the isospin of the pion-nucleon final state, and ξ stands for the magnetic ($\xi = M$), electric ($\xi = E$), and Coulomb or “scalar” ($\xi = S$) transitions,

$$t_{\gamma\pi}^{B,\alpha}(q, k, Q^2) = v_{\gamma\pi}^{B,\alpha}(q, k, Q^2) + \int_0^\infty dq' \frac{q'^2 t_{\pi N}^\alpha(q, q'; W) v_{\gamma\pi}^{B,\alpha}(q', k, Q^2)}{W - W_{\pi N}(q') + i\epsilon}, \quad (12)$$

where $W_{\pi N}(q')$ is the hadronic c.m. energy in the intermediate state. The pion electroproduction potential $v_{\gamma\pi}^{B,\alpha}$ is constructed as in Ref. [6] and contains contributions from the Born terms described by an energy-dependent mixing of pseudovector (PV) and pseudoscalar (PS) πNN coupling as well as t-channel vector meson exchange. The quasi-potential $v_{\gamma\pi}^{B,\alpha}$ depends on 5 parameters: the PV-PS mixing parameter Λ_m as defined in Eq. (12) of Ref. [6] and 4 coupling constants for the vector-meson exchange. The on-shell parts of $v_{\gamma\pi}^{B,\alpha}$ and $t_{\gamma\pi}^{B,\alpha}$ depend on two variables only, i.e.,

$$v_{\gamma\pi}^{B,\alpha}(q, k, Q^2) = v_{\gamma\pi}^{B,\alpha}(W, Q^2) \quad (13)$$

$$t_{\gamma\pi}^{B,\alpha}(q, k, Q^2) = t_{\gamma\pi}^{B,\alpha}(W, Q^2). \quad (14)$$

The Q^2 evolution of the s- and u-channel nucleon pole terms of the background is described by the form factors of Ref. [5]. At the e.m. vertices of the pion-pole and seagull terms we apply a monopole form for the pion form factor and a dipole form for the axial form factor, while the standard dipole form factor is used for the vector-meson exchange.

We note that the background contribution of MAID98 was defined by $t_{\gamma\pi}^{B,\alpha}(\text{MAID98}) = v_{\gamma\pi}^{B,\alpha}(W, Q^2)$ and assumed to be a real and smooth function. The unitarization of the total amplitude was then provided by an additional phase ϕ_α in the resonance contribution such that

the phase of the total amplitude had the phase δ_α of the respective πN scattering state. In MAID2007, however, the background contributions are complex functions defined according to K-matrix theory,

$$t_{\gamma\pi}^{B,\alpha}(W, Q^2) = v_{\gamma\pi}^{B,\alpha}(W, Q^2) [1 + it_{\pi N}^\alpha(W)], \quad (15)$$

where the pion-nucleon elastic scattering amplitudes, $t_{\pi N}^\alpha = [\eta_\alpha \exp(2i\delta_\alpha) - 1]/2i$, are described by the phase shifts δ_α and the inelasticity parameters η_α taken from the GWU/SAID analysis [16]. The assumed structure of the background corresponds to neglecting the principal value integral in the pion-rescattering term of Eq. (12). Our previous studies of the P -wave multipoles in the (3,3) channel [10,15] showed that the “pion cloud” contributions of the principal value integral are effectively included by the dressing of the γNN^* vertex.

Furthermore, the threshold behavior of the S waves was improved. The results of the dynamical approaches [17] show that the pion cloud contributions are very important to obtain a good description of the E_{0+} multipole in the $\pi^0 p$ channel. For this purpose we have introduced the following phenomenological term:

$$E_{0+}^{\text{corr}}(W, Q^2) = \frac{A}{(1 + B^2 q^2)^2} G_D(Q^2), \quad (16)$$

with A and B free parameters fixed by fitting the low-energy π^0 photoproduction data, and G_D the standard nucleon dipole form factor. The threshold correction for the L_{0+} multipole we will consider later in Sect. 5.3. As a result the background contribution of MAID now depends on 8 parameters. We furthermore account for the cusp effect in the $\pi^0 p$ channel appearing at the $\pi^+ n$ threshold by the term [18,19]

$$E_{0+}^{\text{cusp}} = -a_{\pi N} \omega_c \text{Re} E_{0+}^{\gamma\pi^+} \sqrt{1 - \frac{\omega_\pi^2}{\omega_c^2}}, \quad (17)$$

where $\omega_c = 140$ MeV is the π^0 c.m. energy at the cusp and $a_{\pi N} = 0.124/m_{\pi^+}$ the pion charge-exchange amplitude.

3.2 Resonance contributions

For the resonance contributions we follow Ref. [6] and assume Breit-Wigner forms for the resonance shape,

$$t_{\gamma\pi}^{R,\alpha}(W, Q^2) = \bar{\mathcal{A}}_\alpha^R(W, Q^2) \frac{f_{\gamma N}(W) \Gamma_{\text{tot}} M_R f_{\pi N}(W)}{M_R^2 - W^2 - i M_R \Gamma_{\text{tot}}} e^{i\phi_R}, \quad (18)$$

where $f_{\pi N}(W)$ is the usual Breit-Wigner factor describing the decay of a resonance with total width $\Gamma_{\text{tot}}(W)$, partial πN width $\Gamma_{\pi N}$, and spin j ,

$$f_{\pi N}(W) = C_{\pi N} \left[\frac{1}{(2j+1)\pi} \frac{k_W}{q} \frac{m}{M_R} \frac{\Gamma_{\pi N}}{\Gamma_{\text{tot}}^2} \right]^{1/2}, \quad (19)$$

with $C_{\pi N} = \sqrt{3/2}$ and $-1/\sqrt{3}$ for isospin $\frac{3}{2}$ and $\frac{1}{2}$, respectively. The energy dependence of the partial width is given by

$$\Gamma_{\pi N}(W) = \beta_\pi \Gamma_R \left(\frac{q}{q_R} \right)^{2l+1} \left(\frac{X_R^2 + q_R^2}{X_R^2 + q^2} \right)^\ell \frac{M_R}{W}, \quad (20)$$

with $\Gamma_R = \Gamma_{\text{tot}}(M_R)$ and X_R a damping parameter and β_π the single-pion branching ratio. The expression for the total width Γ_{tot} is given in Ref. [6]. The γNN^* vertex is assumed to have the following dependence on W :

$$f_{\gamma N}(W) = \left(\frac{k_W}{k_R} \right)^n \left(\frac{X_R^2 + k_R^2}{X_R^2 + k_W^2} \right), \quad (21)$$

where n is obtained from a best fit to the real photon data, and with the normalization condition $f_{\gamma N}(M_R) = 1$. The phase $\phi_R(W)$ in Eq. (18) is introduced to adjust the total phase such that the Fermi-Watson theorem is fulfilled below two-pion threshold. For the S - and P -wave multipoles we extend this unitarization procedure up to $W = 1400$ MeV. Because of a lack of further information, we assume that the phases ϕ_R are constant at the higher energies. In particular we note that the phase ϕ_R for the $P_{33}(1232)$ excitation vanishes at $W = M_R = 1232$ MeV for all values of Q^2 . For this multipole we may even apply the Fermi-Watson theorem up to $W \approx 1600$ MeV because the inelasticity parameter η_α remains close to 1. For the D - and F -wave resonances, the phases ϕ_R are assumed to be constant and determined from the best fit.

Whereas MAID98 [6] included only the 7 most important nucleon resonances, essentially with only transverse e.m. couplings, our present version contains all 13 resonances of the 4-star tier below 2 GeV with transverse electric ($\bar{\mathcal{A}}_\alpha^R = \bar{E}_{l\pm}$), transverse magnetic ($\bar{\mathcal{A}}_\alpha^R = \bar{M}_{l\pm}$), and Coulomb ($\bar{\mathcal{A}}_\alpha^R = \bar{S}_{l\pm}$) couplings: $P_{33}(1232)$, $P_{11}(1440)$, $D_{13}(1520)$, $S_{11}(1535)$, $S_{31}(1620)$, $S_{11}(1650)$, $D_{15}(1675)$, $F_{15}(1680)$, $D_{33}(1700)$, $P_{13}(1720)$, $F_{35}(1905)$, $P_{31}(1910)$, and $F_{37}(1950)$. Because we determine the isovector amplitudes from the proton channels, the number of the e.m. couplings is 34 for the proton and 18 for the neutron channels, that is 52 parameters altogether. These are taken to be constant in a single- Q^2 analysis, e.g., in photoproduction but also at any fixed Q^2 if sufficient data are available in the chosen energy and angular range. Alternatively, the couplings have also been parameterized as functions of Q^2 , as is discussed in Sec. 5.

The more commonly used helicity amplitudes $A_{1/2}$, $A_{3/2}$, and $S_{1/2}$ are given by linear combinations of the e.m. couplings $\bar{\mathcal{A}}_\alpha^R$. These relations take the form

$$\begin{aligned} A_{1/2}^{\ell+} &= -\frac{1}{2}[(\ell+2)\bar{E}_{\ell+} + \ell\bar{M}_{\ell+}], \\ A_{3/2}^{\ell+} &= \frac{1}{2}\sqrt{\ell(\ell+2)}(\bar{E}_{\ell+} - \bar{M}_{\ell+}), \\ S_{1/2}^{\ell+} &= -\frac{\ell+1}{\sqrt{2}}\bar{S}_{\ell+} \end{aligned} \quad (22)$$

Table 1. The reduced e.m. amplitudes $\bar{\mathcal{A}}_\alpha$ defined by Eq. (18) in terms of the helicity amplitudes.

N^*	E	M	S
S_{11}/S_{31}	$-A_{1/2}$	—	$-\sqrt{2}S_{1/2}$
P_{13}/P_{33}	$\frac{1}{2}(\frac{1}{\sqrt{3}}A_{3/2} - A_{1/2})$	$-\frac{1}{2}(\sqrt{3}A_{3/2} + A_{1/2})$	$-\frac{1}{\sqrt{2}}S_{1/2}$
P_{11}/P_{31}	—	$A_{1/2}$	$-\sqrt{2}S_{1/2}$
D_{13}/D_{33}	$-\frac{1}{2}(\sqrt{3}A_{3/2} + A_{1/2})$	$-\frac{1}{2}(\frac{1}{\sqrt{3}}A_{3/2} - A_{1/2})$	$-\frac{1}{\sqrt{2}}S_{1/2}$
D_{15}/D_{35}	$\frac{1}{3}(\frac{1}{\sqrt{2}}A_{3/2} - A_{1/2})$	$-\frac{1}{3}(\sqrt{2}A_{3/2} + A_{1/2})$	$-\frac{\sqrt{2}}{3}S_{1/2}$
F_{15}/F_{35}	$-\frac{1}{3}(\sqrt{2}A_{3/2} + A_{1/2})$	$-\frac{1}{3}(\frac{1}{\sqrt{2}}A_{3/2} - A_{1/2})$	$-\frac{\sqrt{2}}{3}S_{1/2}$
F_{17}/F_{37}	$\frac{1}{4}(\sqrt{\frac{3}{5}}A_{3/2} - A_{1/2})$	$-\frac{1}{4}(\sqrt{\frac{5}{3}}A_{3/2} + A_{1/2})$	$-\frac{1}{2\sqrt{2}}S_{1/2}$

for resonances with total spin $j = \ell + \frac{1}{2}$, and

$$\begin{aligned}
A_{1/2}^{\ell-} &= \frac{1}{2}[(\ell+1)\bar{M}_{\ell-} - (\ell-1)\bar{E}_{\ell-}], \\
A_{3/2}^{\ell-} &= -\frac{1}{2}\sqrt{(\ell-1)(\ell+1)}(\bar{E}_{\ell-} + \bar{M}_{\ell-}), \\
S_{1/2}^{\ell-} &= -\frac{\ell}{\sqrt{2}}\bar{S}_{\ell-}
\end{aligned} \quad (23)$$

for total spin $j = \ell - \frac{1}{2}$. The inverse relations for the partial waves are listed in Table 1. The helicity amplitudes are related to matrix elements of the e.m. current J_μ between the nucleon and the resonance states, e.g., as obtained in the framework of quark models,

$$\begin{aligned}
A_{1/2} &= -\sqrt{\frac{2\pi\alpha_{\text{em}}}{k_W}} < R, \frac{1}{2} | J_+ | N, -\frac{1}{2} > \zeta, \\
A_{3/2} &= -\sqrt{\frac{2\pi\alpha_{\text{em}}}{k_W}} < R, \frac{3}{2} | J_+ | N, \frac{1}{2} > \zeta, \\
S_{1/2} &= -\sqrt{\frac{2\pi\alpha_{\text{em}}}{k_W}} < R, \frac{1}{2} | \rho | N, \frac{1}{2} > \zeta,
\end{aligned} \quad (24)$$

where $J_+ = -\frac{1}{\sqrt{2}}(J_x + iJ_y)$ and $\alpha_{\text{em}} = 1/137$. However, these equations define the couplings only up to a phase ζ , which in principle can be obtained from the pionic decay of the resonance calculated within the same model. Because this phase is ignored in most of the literature, the comparison of the sign is not always meaningful, especially in critical cases such as the Roper resonance whose correct sign is not obvious from the data. In contrast with MAID98 and MAID2000, our present version uses the helicity amplitudes $A_{1/2}$, $A_{3/2}$, and $S_{1/2}$ for photoproduction as input parameters, except for the $P_{33}(1232)$ resonance which is directly described by the 3 e.m. amplitudes $\bar{\mathcal{A}}_\alpha$.

4 Partial-wave analysis of pion photoproduction data

The unitary isobar model MAID2007 has been developed to analyze the world data of pion photo- and electroproduction. In this section we fix (I) the background parameters and the helicity amplitudes for pion photoproduction ($Q^2 = 0$) and (II) the dependence of the resonance contributions on the c.m. energy W . These results are then generalized to pion electroproduction in the next section.

4.1 Data base for pion photoproduction and fit procedure

The main part of the photoproduction data was taken from the GWU/SAID compilation of SAID2000, which includes the data published between 1960 and 2000, a total of 14700 data points. A separation of these data in different physical channels and observables is given in Table 2. In the following years the data base was extended by including recent results from MAMI (Mainz) [20, 21, 22, 23], GRAAL (Grenoble) [24, 25], LEGS (Brookhaven) [26], and ELSA (Bonn) [27] as listed in Table 3. Altogether 4976 more data points were added. As a result our full data base contains 19676 points within the energy range $140 \text{ MeV} < E_\gamma < 1610 \text{ MeV}$.

Table 2. Number of data points from the SAID2000 data base for differential cross sections ($d\sigma$), photon asymmetries (Σ), target asymmetries (T), and recoil asymmetries (P).

channel	$d\sigma$	Σ	T	P	total
$n\pi^+$	4646	760	645	205	6256
$p\pi^0$	4936	673	353	540	6502
$p\pi^-$	1554	206	94	88	1942

Table 3. Number of data points collected after 2000 for differential cross sections ($d\sigma$), photon asymmetries (Σ), and helicity asymmetries $\Delta\sigma = d\sigma_{1/2} - d\sigma_{3/2}$.

channel	range E_γ (MeV)	data points (observable)	Ref.
$p\pi^0$	202-790	1129 ($d\sigma$) + 357 (Σ)	[20]
$p\pi^0$	310-780	174 ($d\sigma$) + 138 ($\Delta\sigma$)	[21]
$p\pi^+$	180-450	205 ($d\sigma$) + 129 ($\Delta\sigma$)	[22]
$p\pi^+$	463-783	204 ($d\sigma$) + 102 ($\Delta\sigma$)	[23]
$p\pi^+$	800-1454	237 (Σ)	[24]
$p\pi^0$	555-1541	861 ($d\sigma$) + 469 (Σ)	[25]
$n\pi^-$	285-769	300 ($d\sigma$)	[26]
$p\pi^0$	513-1575	671 ($d\sigma$)	[27]
total		4976	

Our strategy for the data analysis is as follows. First, we try to find a global (energy dependent) solution by fitting all the data in the range $140 \text{ MeV} \leq E_\gamma \leq 1610 \text{ MeV}$. This allows us to determine the phase of the multipoles, i.e., the ratio $\text{Im} t_{\gamma\pi}^\alpha / \text{Re} t_{\gamma\pi}^\alpha$ above the two-pion threshold. At the lower energies this phase is constrained by the πN scattering phase. In a second step we perform local (single energy) fits to the data, in energy bins of 10 MeV in the range $140 \text{ MeV} \leq E_\gamma \leq 460 \text{ MeV}$ and of 20 MeV for the higher energies, by varying the absolute values of the multipoles but keeping the phase as previously determined. Similar to the prescription of the SAID group we minimize the modified χ^2 function

$$\chi^2 = \sum_i^{N_{\text{data}}} \left(\frac{\Theta_i - \Theta_i^{\text{exp}}}{\delta\Theta_i} \right)^2 + \sum_j^{N_{\text{mult}}} \left(\frac{X_j - 1}{\Delta} \right)^2. \quad (25)$$

The first term on the r.h.s. of this equation is the standard χ^2 function with Θ_i the calculated and Θ_i^{exp} the measured observables, $\delta\Theta_i$ the statistical errors, and N_{data} the number of data points. In the second term, N_{mult} is the number of the varied multipoles and X_j describes the deviation from the global fit. The fitting procedure starts with the initial value $X_j = 1$ corresponding to the global solution, and the quantity Δ enforces a smooth energy dependence of the single-energy solution. In the limit of $\Delta \rightarrow \infty$ we obtain the standard χ_{std}^2 , and for $\Delta \rightarrow 0$ the single-energy and the global solutions become identical. The optimum value for Δ is chosen from the condition $1 < \chi^2/\chi_{\text{std}}^2 < 1.05$. The described two-step fitting procedure can be repeated several times by adjusting the energy dependence of the global solution, for example by changing the parameters X_R and n in Eqs. (20-21) in order to improve the agreement between the global and local solutions.

4.2 Results for pion photoproduction

Our results for χ^2 are summarized in Table 4 by comparing the local and global solutions for different energy ranges and channels. We recall that the number of varied multipoles N_{mult} in the proton and neutron channels is different. Since the number of data points in the proton channels ($\gamma\pi^0$ and $\gamma\pi^+$) is about one order of magnitude larger than for the neutron channel ($\gamma\pi^-$), we proceed as follows. First, we analyze the proton channel and extract the multipoles ${}_pE_{l\pm}^{1/2}$, ${}_pM_{l\pm}^{1/2}$, $E_{l\pm}^{3/2}$, and $M_{l\pm}^{3/2}$ as defined in Ref. [6]. Second, with the thus obtained values for the isospin 3/2 multipoles, we extract the multipoles ${}_nE_{l\pm}^{1/2}$ and ${}_nM_{l\pm}^{1/2}$ from the neutron channel. In this way we minimize the pressure from the large number of proton data on the results in the neutron channel. The number of varied multipoles also depends on the energy. For $E_\gamma < 450 \text{ MeV}$ we vary all the S - and P -wave multipoles plus ${}_p,nE_{2-}^{1/2}$ and $E_{2-}^{3/2}$. At the higher energies we include all the multipoles up to the F waves.

Table 4. Results for χ^2 from single-energy (se) and global (gl) solutions.

$E_\gamma [\text{MeV}]$	proton			
	N_{mult}	N_{data}	χ_{se}^2	χ_{gl}^2
140—200	10	990	787	2346
200—450	10	5622	5454	14236
450—850	24	6403	6996	22700
850—1210	24	2965	4133	24990
1210—1610	24	1454	4737	12594
total		17434	22107	76866
$E_\gamma [\text{MeV}]$	neutron			
	N_{mult}	N_{data}	χ_{se}^2	χ_{gl}^2
140—200	5	51	113	151
200—450	5	872	1613	2203
450—850	12	902	1748	3414
850—1210	12	334	651	2311
1210—1610	12	83	107	583
total		2242	4222	9262

The best fit for the background and the resonance parameters yields the results listed in Tables 5 and 6, respectively. The PS-PV mixing parameter and the vector-meson coupling constants are defined as in Ref. [6]. However we note that in the present version we do not use form factors at the hadronic vertices involving vector-meson exchange. In Tables 7 and 8 we com-

Table 5. Masses and coupling constants for vector mesons, PS-PV mixing parameter Λ_m , and parameter A for the low-energy correction of Eq. (16).

	$m_V [\text{MeV}]$	λ_V	\tilde{g}_{V1}	$\tilde{g}_{V2}/\tilde{g}_{V1}$
ω	783	0.314	16.3	-0.94
ρ	770	0.103	1.8	12.7
$\Lambda_m = 423 \text{ MeV}$		$A = 1.9 \times 10^{-3}/m_\pi^+$		$B = 0.71 fm$

pare the helicity amplitudes obtained from MAID2003 and MAID2007 with the results of the PDG [2] and GWU/SAID [28,29] analysis. As is very typical for a global analysis with about 20,000 data points fitted to a small set of 20-30 parameters, the fit errors appear unrealistically small. However, one should realize that these errors only reflect the statistical uncertainty of the experimental error, whereas the model uncertainty can be larger by an order of magnitude. We therefore do not list our fit errors, which in fact are very similar in the GW02 or GW06 fits of the SAID group [28,29]. The only realistic error estimate is obtained by comparing different analysis, such as SAID, MAID, and coupled-channels approaches.

Next we present our results for the multipoles starting with the threshold region. In Fig. 1 we demonstrate the effects of the low-energy correction and the cusp

Table 6. Resonance masses M_R , widths Γ_R , single-pion branching ratios β_π , and angles ϕ_R as well as the parameters X_R, n_E , and n_M of the vertex function Eq. (21).

N^*	$M_R[\text{MeV}]$	$\Gamma_R[\text{MeV}]$	β_π	$\phi_R[\text{deg}]$	$X_R[\text{MeV}]$	proton		neutron	
						n_E	n_M	n_E	n_M
$P_{33}(1232)$	1232	130	1.0	0.0	570	-1	2	-1	2
$P_{11}(1440)$	1440	350	0.70	-15	470	—	0	—	-1
$D_{13}(1520)$	1530	130	0.60	32	500	3	4	7	2
$S_{11}(1535)$	1535	100	0.40	8.2	500	2	—	2	—
$S_{31}(1620)$	1620	150	0.25	23	470	5	—	5	—
$S_{11}(1650)$	1690	100	0.85	7.0	500	4	—	4	—
$D_{15}(1675)$	1675	150	0.45	20	500	3	5	3	4
$F_{15}(1680)$	1680	135	0.70	10	500	3	3	2	2
$D_{33}(1700)$	1740	450	0.15	61	700	4	5	4	5
$P_{13}(1720)$	1740	250	0.20	0.0	500	3	3	3	3
$F_{35}(1905)$	1905	350	0.10	40	500	4	5	4	5
$P_{31}(1910)$	1910	250	0.25	35	500	—	1	—	1
$F_{37}(1950)$	1945	280	0.40	30	500	6	6	6	6

Table 7. Proton helicity amplitudes at $Q^2 = 0$ for the major nucleon resonances, in units $10^{-3} \text{ GeV}^{-1/2}$. The results with MAID2003 and MAID2007 are compared to the PDG [2] and GWU/SAID [29] analysis.

		PDG	GW06	2003	2007
$P_{33}(1232)$	$A_{1/2}$	-135±6	-139.1±3.6	-140	-140
	$A_{3/2}$	-250±8	-257.6±4.6	-265	-265
$E2/M1$ (%)		-2.5±0.5		-2.2	-2.2
$P_{11}(1440)$	$A_{1/2}$	-65 ±4	-50.6 ±1.9	-77	-61
$D_{13}(1520)$	$A_{1/2}$	-24 ±9	-28.0 ±1.9	-30	-27
	$A_{3/2}$	166 ±5	143.1 ±2.0	166	161
$S_{11}(1535)$	$A_{1/2}$	90 ±30	91.0 ±2.2	73	66
$S_{31}(1620)$	$A_{1/2}$	27 ±11	49.6±2.2	71	66
$S_{11}(1650)$	$A_{1/2}$	53±16	22.2 ±7.2	32	33
$D_{15}(1675)$	$A_{1/2}$	19 ±8	18.0 ±2.3	23	15
	$A_{3/2}$	15 ±9	21.2 ±1.4	24	22
$F_{15}(1680)$	$A_{1/2}$	-15 ±6	-17.3 ±1.4	-25	-25
	$A_{3/2}$	133 ±12	133.6 ±1.6	134	134
$D_{33}(1700)$	$A_{1/2}$	104 ±15	125.4 ±3.0	135	226
	$A_{3/2}$	85 ±22	105.0 ±3.2	213	210
$P_{13}(1720)$	$A_{1/2}$	18 ±30	96.6 ±3.4	55	73
	$A_{3/2}$	-19 ±20	-39.0 ±3.2	-32	-11
$F_{35}(1905)$	$A_{1/2}$	26 ±11	21.3 ±3.6	14	18
	$A_{3/2}$	-45 ±20	-45.6±4.7	-22	-28
$F_{37}(1950)$	$A_{1/2}$	-76 ±12		-78	-94
	$A_{3/2}$	-97 ±10		-101	-121

effect for π^0 photoproduction, as described by Eqs. (16) and (17), respectively. The prediction of MAID98 for π^0 photoproduction at threshold (dotted lines) lies substantially below the data. In accordance with Ref. [17], the phenomenological term E_{0+}^{corr} simulates the pion off-shell rescattering or pion-loop contributions of ChPT. The cusp term of Eq. (17) describes the strong energy dependence near π^+ threshold, which has its origin in the pion mass difference and the strong coupling with

Table 8. Neutron helicity amplitudes at $Q^2 = 0$ for the major nucleon resonances. GW02 are the results GWU/SAID analysis [28]. Further notation as in Tab. 7.

		PDG	GW02	2003	2007
$P_{11}(1440)$	$A_{1/2}$	40±10	47±5	52	54
$D_{13}(1520)$	$A_{1/2}$	-59 ±9	-67 ±4	-85	-77
	$A_{3/2}$	-139 ±11	-112 ±3	-148	-154
$S_{11}(1535)$	$A_{1/2}$	-46±27	-16±5	-42	-51
$S_{11}(1650)$	$A_{1/2}$	-15±21	-28±4	27	9
$D_{15}(1675)$	$A_{1/2}$	-43 ±12	-50 ±4	-61	-62
	$A_{3/2}$	-58 ±13	-71 ±5	-74	-84
$F_{15}(1680)$	$A_{1/2}$	29 ±10	29 ±6	25	28
	$A_{3/2}$	-33 ±9	-58 ±9	-35	-38
$P_{13}(1720)$	$A_{1/2}$	1 ±15		17	-3
	$A_{3/2}$	-29 ±61		-75	-31

the π^+n channel. The figure shows that the off-shell pion rescattering substantially improves the agreement with the data. However, one problem still remains in the threshold region. The experimental photon asymmetry Σ in π^0 photoproduction at $E_\gamma \approx 160 \text{ MeV}$ takes positive values, whereas the MAID results are negative in this region. As has been demonstrated in Refs. [17,32], this observable is very sensitive to the M_{1-} multipole which strongly depends on the details of the low-energy behavior of Roper resonance, vector meson and off-shell pion rescattering contributions. Therefore, a slight modification of one or all of these mechanisms can drastically change the photon asymmetry.

Figures 2-4 display the results for the most important S and P waves in the $\Delta(1232)$ region. However, a look at Fig. 5 shows that also the D -wave amplitudes ${}_pE_{2-}^{1/2}$, $E_{2-}^{3/2}$, and ${}_nE_{2-}^{1/2}$, give sizable contributions in this region, in particular through their real parts. In these figures, we present the MAID and SAID global (energy dependent)

solutions, together with our local (single energy) fit obtained for energy bins of 10 MeV. In general the MAID and SAID results are close, which is not too surprising because the phases are constrained by the Fermi-Watson theorem. However, there are much larger differences in the ${}_pE_{0+}^{1/2}$ and ${}_pE_{2-}^{1/2}$ amplitudes, which indicates that the present data base is still too limited to determine these background amplitudes in a reliable way.

More substantial discrepancies between the MAID and SAID analyses are found in the second and third resonance regions. A detailed comparison of the two models is shown in Figs. 6-13. As pointed out in Sect. 3.1, it is prerequisite to know the phases of the multipoles in order to get correct single-energy solutions above the two-pion threshold. In MAID2007 these phases are determined by Eqs. (9), (15), and (18). The SAID analysis is based on the following parametrization of the partial wave amplitudes:

$$t_{\gamma\pi} = (\text{Born} + A)(1 + it_{\pi N}) + B t_{\pi N} + (C + iD)(\text{Im } t_{\pi N} - |t_{\pi N}|^2), \quad (26)$$

where A , B , C and D are polynomials in the energy with real coefficients, and $t_{\pi N}$ is the pion-nucleon elastic scattering amplitude of Eq. (15). As seen in the first resonance region, the most serious differences between MAID and SAID are again found for the real parts of the multipoles ${}_pE_{0+}^{1/2}$ and ${}_pE_{2-}^{1/2}$. We have checked the phases of these multipoles by independent calculations on the basis of dispersion relations [33,34]. The result confirmed our phase relations. Concerning the small amplitudes, the most sizable differences between SAID and MAID are in the $M_{1-}^{3/2}$, ${}_pM_{1+}^{1/2}$ and ${}_pE_{1+}^{1/2}$ multipoles. In the neutron channel, the largest differences are in the multipoles ${}_nE_{0+}^{1/2}$, ${}_nE_{3-}^{1/2}$, ${}_nE_{1+}^{1/2}$, and ${}_nM_{1+}^{1/2}$. In the last two cases this is due to the large contribution from the $P_{13}(1720)$ resonance which is not found in the SAID analysis (see Table 7).

Let us finally discuss the possible contributions of the weaker resonances. As discussed in Ref. [35], the two additional S_{11} resonances found with masses of about 1800 and 2000 MeV might also show up in pion photoproduction. This conclusion was mainly based on the single-energy solution of the SAID group. As illustrated by Fig. 14, our present analysis requires only one additional S_{11} resonance with mass $M_R \approx 1950$ MeV, and our single-energy solution shows no resonance at $M_R \approx 1800$ MeV. Of course, the solution of the problem is certainly correlated with the way how the resonance and background contributions are separated. As demonstrated both in Ref. [35] and by Fig. 6, the background is very important for this particular channel. In this context we recall that we use the same form of the unitarized background contribution (Born, ω and ρ exchange) for all the partial waves. Another interesting topic deserving further experimental and theoretical studies, concerns the Roper or P_{11} channel. As clearly seen in Fig. 15, both our and the SAID analysis yield a second resonance structure of the ${}_pM_{1-}^{1/2}$ mul-

tipole at $E_\gamma \approx 1070$ MeV or $W \approx 1700$ MeV. However, our analysis yields a very small width of $\Gamma_{\text{tot}} \approx 30$ -60 MeV, whereas the PDG lists $\Gamma_{\text{tot}} \approx 50$ -250 MeV for this resonance. Moreover, also the helicity amplitude differs, whereas our result is $A_{1/2} \approx -0.024 \text{ GeV}^{-1/2}$, the PDG lists $0.009 \pm 0.022 \text{ GeV}^{-1/2}$. Of course, these numbers do strongly depend on the values for the single-pion branching ratio. On the other hand, we do not anticipate large effects from different definitions of the background in this channel, because the background contribution is very small in the resonance region (see Fig. 7).

5 Partial-wave analysis of pion electroproduction

In most of the pion electroproduction experiments the five-fold differential cross section was measured. However, different conventions exist for the partial cross sections, and therefore we recall the definitions used in MAID. For an unpolarized target the cross sections written as the product of the virtual-photon flux factor Γ_v and the virtual photon cross section $d\sigma_v/d\Omega_\pi$ [36],

$$\frac{d\sigma}{d\Omega_f^L dE_f^L d\Omega_\pi} = \Gamma_v \frac{d\sigma_v}{d\Omega_\pi}, \quad (27)$$

$$\begin{aligned} \frac{d\sigma_v}{d\Omega_\pi} &= \frac{d\sigma_T}{d\Omega_\pi} + \epsilon \frac{d\sigma_L}{d\Omega_\pi} + \sqrt{2\epsilon(1+\epsilon)} \frac{d\sigma_{LT}}{d\Omega_\pi} \cos \Phi_\pi \\ &+ \epsilon \frac{d\sigma_{TT'}}{d\Omega_\pi} \cos 2\Phi_\pi + h \sqrt{2\epsilon(1-\epsilon)} \frac{d\sigma_{LT'}}{d\Omega_\pi} \sin \Phi_\pi, \end{aligned} \quad (28)$$

where ϵ and h describe the polarizations of the virtual photon and the electron, respectively. We further note that the hadronic kinematics is expressed in the c.m. system, whereas the electron and virtual photon kinematics is written in the lab frame, as indicated by L in the following variables: the initial and final electron energies E_i^L and E_f^L , respectively, the electron scattering angle θ_L , the photon energy $\omega_L = E_i^L - E_f^L$, and the photon three-momentum \mathbf{k}_L . With these definitions the virtual photon flux and the transverse photon polarization take the form

$$\epsilon = \frac{1}{1 + 2 \frac{\mathbf{k}_L^2}{Q^2} \tan^2 \frac{\theta_L}{2}}, \quad \Gamma_v = \frac{\alpha_{\text{em}}}{2\pi^2} \frac{E_f^L}{E_i^L} \frac{K}{Q^2} \frac{1}{1-\epsilon}. \quad (29)$$

As in our previous notation [36], the flux is denoted by the photon “equivalent energy” in the lab frame, $K = K_H = (W^2 - m^2)/2m$ as originally introduced by Hand [37]. Another definition was given by Gilman [38] who used $K = K_G = |\mathbf{k}_L|$.

The first two terms on the r.h.s. of Eq. (28) are the transverse (T) and longitudinal (L) cross sections. They do not depend on the pion azimuthal angle Φ_π . The third and fifth terms describe longitudinal-transverse interferences (LT , LT'). They contain an explicit factor $\sin \theta_\pi$ and

therefore are vanishing along the axis of momentum transfer. The same is true for the fourth term, a transverse-transverse interference (TT) proportional to $\sin^2 \theta_\pi$. It is useful to express these 5 cross sections in terms of hadronic response functions depending only on 3 independent variables, i.e., $R_i = R_i(Q^2, W, \theta_\pi)$. The corresponding relations take the form

$$\frac{d\sigma_T}{d\Omega_\pi} = \frac{q}{k_W} R_T, \quad \frac{d\sigma_{TT}}{d\Omega_\pi} = \frac{q}{k_W} R_{TT}, \quad \frac{d\sigma_L}{d\Omega_\pi} = \frac{q}{k_W} \frac{Q^2}{\omega_\gamma^2} R_L,$$

$$\frac{d\sigma_{LT}}{d\Omega_\pi} = \frac{q}{k_W} \frac{Q}{\omega_\gamma} R_{LT}, \quad \frac{d\sigma_{LT'}}{d\Omega_\pi} = \frac{q}{k_W} \frac{Q}{\omega_\gamma} R_{LT'}. \quad (30)$$

As a result of this equation, the longitudinal (L) and longitudinal-transverse (LT and LT') response functions must be proportional to ω_γ^2 and ω_γ , respectively, in order to avoid non-physical singularities at the energy for which the c.m. virtual photon energy passes through zero. The 5 response functions may be expressed in terms of 6 independent CGLN amplitudes F_1, \dots, F_6 [39], or in terms of the helicity amplitudes H_1, \dots, H_6 , which are linear combinations of the CGLN amplitudes. The relevant expressions can be found in Refs. [36, 40].

5.1 Data base for pion electroproduction and fit procedure

The main part of our data base for pion electroproduction includes the compilation of the GWU/SAID group [41] in 2000 and recent data from Bonn and JLab (see Table 9). Altogether this base contains about 70000 data points within the energy range $1.074 \text{ GeV} < W < 2 \text{ GeV}$ and photon virtuality range $0.1 \text{ GeV}^2 \leq Q^2 \leq 6 \text{ GeV}^2$. In addition we have analyzed high precision data from Bates [47, 48], Mainz [49, 50], and JLab [5, 51]. Our fitting procedure was as follows. In a first step we fitted the data sets at constant values of Q^2 (single- Q^2 fit). This procedure is similar to the partial-wave analysis for pion photoproduction except for the additional longitudinal couplings of the resonances. Second, we introduced a smooth Q^2 evolution of the e.m. transition form factors and parameterized the 3 helicity amplitudes accordingly. In a combined fit with the complete electroproduction data base and information from the single- Q^2 fits we finally constructed the Q^2 -dependent solution (super-global fit). This new solution (MAID2007) was then compared with the previous solution (MAID2003) in terms of χ^2 as presented in Table 9. In most cases the new fit improves the description of the data, in particular for the $n\pi^+$ channel.

5.2 Results for the $\Delta(1232)$ form factors

In the literature the e.m. properties of the $N\Delta(1232)$ transition are described by either the magnetic (G_M^*), electric (G_E^*), and Coulomb (G_C^*) form factors or the helicity amplitudes $A_{1/2}$, $A_{3/2}$, and $S_{1/2}$, which can be derived from

Table 9. The number of data points, N_{data} , and the χ^2 value per data point obtained with MAID2003 and MAID2007.

Ref. channel	W (MeV) Q^2 (GeV 2)	N_{data} observables	χ^2/N_{data} (2003) χ^2/N_{data} (2007)
SAID00 $p\pi^0$	1074-1895 0.1-4.3	13152 $d\sigma, \dots$	3.238 3.172
SAID00 $n\pi^+$	1125-1975 0.117-4.4	5464 $d\sigma, \dots$	3.297 4.188
Bonn02 [42] $p\pi^0$	1153-1312 0.63	4914 $d\sigma$	1.378 1.400
CLAS02 [43] $p\pi^0$	1110-1680 0.4-1.80	31810 $d\sigma$	1.907 1.952
CLAS03 [44] $p\pi^0$	1100-1660 0.4-0.65	223 $d\sigma_{LT'}$	4.881 3.490
CLAS04 [45] $n\pi^+$	1100-1660 0.4-0.65	224 $d\sigma_{LT'}$	4.879 2.196
CLAS06 [46] $n\pi^+$	1110-1570 0.3-0.60	4179 $d\sigma$	10.04 4.954
CLAS06 [13] $p\pi^0$	1110-1390 3.0-6.0	8491 $d\sigma$	1.691 1.335
total $p\pi^0, n\pi^+$	1074-1975 0.1-6.0	68457 $d\sigma, \dots$	2.724 2.437
SAID00 $p\pi^-$	1253-1976 0.54-1.36	799 $d\sigma$	2.100 2.264

the reduced e.m. amplitudes $\bar{\mathcal{A}}_\alpha$ as defined by Eq. (18). It is worthwhile pointing out that these amplitudes are related to the multipoles over the full energy region, that is, they are the primary target of the fitting procedure. The form factors and helicity amplitudes are then obtained by evaluating the reduced e.m. amplitudes at the resonance position $W = M_\Delta = 1232 \text{ MeV}$. The respective relations take the following form:

$$G_M^*(Q^2) = -c_\Delta(A_{1/2} + \sqrt{3}A_{3/2}) = 2c_\Delta \bar{\mathcal{A}}_M^\Delta(M_\Delta, Q^2),$$

$$G_E^*(Q^2) = c_\Delta(A_{1/2} - \frac{1}{\sqrt{3}}A_{3/2}) = -2c_\Delta \bar{\mathcal{A}}_E^\Delta(M_\Delta, Q^2),$$

$$G_C^*(Q^2) = \sqrt{2}c_\Delta \frac{2M_\Delta}{k_\Delta} S_{1/2} = -2c_\Delta \frac{2M_\Delta}{k_\Delta} \bar{\mathcal{A}}_S^\Delta(M_\Delta, Q^2),$$

with $c_\Delta = \left(\frac{m^3 k_W^\Delta}{4\pi\alpha_{\text{em}} M_\Delta k_\Delta^2} \right)^{1/2}$, (31)

and where $k_\Delta = k_\Delta(Q^2) = k(M_\Delta, Q^2)$ and $k_W^\Delta = k(M_\Delta, 0)$ are the virtual photon momentum and the photon equivalent energy at resonance. Because the $\Delta(1232)$ is very close to an ideal resonance, the real part of the amplitudes vanishes for $W = M_\Delta$ and the form factors can be directly expressed by the imaginary parts of the corresponding multipoles at the resonance position,

$$G_M^*(Q^2) = b_\Delta \text{Im}\{M_{1+}^{(3/2)}(M_\Delta, Q^2)\},$$

$$G_E^*(Q^2) = -b_\Delta \text{Im}\{E_{1+}^{(3/2)}(M_\Delta, Q^2)\}, \quad (32)$$

$$G_C^*(Q^2) = -b_\Delta \frac{2M_\Delta}{k_\Delta} \text{Im}\{S_{1+}^{(3/2)}(M_\Delta, Q^2)\},$$

$$\text{where } b_\Delta = \left(\frac{8 m^2 q_\Delta \Gamma_\Delta}{3 \alpha_{\text{em}} k_\Delta^2} \right)^{1/2},$$

and with $\Gamma_\Delta = 115$ MeV and $q_\Delta = q(M_\Delta)$ the pion momentum at resonance. The above definition of the form factors is due to Ash [52]. The form factors of Jones and Scadron [53] are obtained by multiplying our form factors with $\sqrt{1 + Q^2/(M_N + M_\Delta)^2}$. We note that the form factor G_C^* differs from our previous work [54] by the factor $2M_\Delta/k_\Delta$ in Eq. (32). With these definitions all 3 transition form factors remain finite at pseudo-threshold (Siegert limit). In the literature, the following ratios of multipoles have been defined:

$$R_{EM} = -\frac{G_E^*}{G_M^*} = \frac{A_{1/2} - \frac{1}{\sqrt{3}}A_{3/2}}{A_{1/2} + \sqrt{3}A_{3/2}}, \quad (33)$$

$$R_{SM} = -\frac{k_\Delta}{2M_\Delta} \frac{G_C^*}{G_M^*} = \frac{\sqrt{2}S_{1/2}}{A_{1/2} + \sqrt{3}A_{3/2}}. \quad (34)$$

In MAID2003 the Q^2 dependence of the e.m. amplitudes \bar{A}_α^Δ was parameterized as follows:

$$\bar{A}_\alpha^\Delta(W, Q^2) = A_\alpha^0(1 + \beta_\alpha Q^{2n_\alpha}) \frac{k}{k_W} e^{-\gamma_\alpha Q^2} G_D(Q^2), \quad (35)$$

where $G_D(Q^2) = 1/(1 + Q^2/0.71 \text{ GeV}^2)^2$ is the dipole form factor. MAID2007 follows this parametrization for the magnetic and electric amplitudes, although with somewhat different values of the parameters (see Table 10). In order to fulfill the Siegert theorem, we have however changed the description of the Coulomb amplitude as specified below. The results of MAID2003 and MAID2007

Table 10. Parameters for the $N\Delta$ amplitudes given by Eqs. (35) and (42). The amplitudes A_α^0 are in units $10^{-3} \text{ GeV}^{-1/2}$, the parameters β and γ in GeV^{-2} . For the Coulomb amplitude in MAID2007 we use Eq. (42) with $d=4.9$.

	M	E	S	model
A_α^0	300	-6.50	-19.50	2003
	300	-6.37	-12.40	2007
β_α	0	-0.306	0.017	2003
	0.01	-0.021	0.12	2007
γ_α	0.21	0.21	0.21	2003
	0.23	0.16	0.23	2007
n_α	1	1	3	2003
	1	1	—	2007

for $G_M^*(Q^2)$ are compared in Fig. 16. Because our single- Q^2 analysis follows the global fit closely, it is not shown in the figure. We find an excellent agreement with the data, which also include the new high- Q^2 data of the JLab/CLAS Collaboration [13]. At this point a word of caution is in order. Because the form factors are extracted from the multipoles by Eq. (32), they are proportional to $\sqrt{T_\Delta}$. The MAID fit to the experimental data yields

$\Gamma_\Delta=130$ MeV, which is different from the usually assumed value of about 115 MeV. Therefore, in order to compare with form factor values of other analyses, we scale our predicted form factor with $\sqrt{115/130}$. As shown in Fig. 16, $G_M^*(0)/3$ will then take the usual value of 1 to an accuracy of 1%. From this number we can determine the $N \rightarrow \Delta$ magnetic transition moment, $\mu_{N\Delta} = 3.46 \pm 0.03$, in units of the nuclear magneton.

5.3 Siegert theorem and ratios R_{EM} and R_{SM}

Let us next discuss our results for the R_{EM} and R_{SM} ratios. In all previous solutions these ratios were nearly constant for $Q^2 < 1 \text{ GeV}^2$. However, calculations in effective field theories [55,56] and dynamical models [10, 15,57] indicated a rapid rise of R_{SM} for $Q^2 \rightarrow +0$. This dependence is rather model-independent, because it reflects the behavior of the multipoles at physical threshold (pion momentum $\mathbf{q} \rightarrow 0$) and pseudothreshold (Siegert limit, photon momentum $\mathbf{k} \rightarrow 0$) [58]. The longitudinal and Coulomb multipoles are related by gauge invariance, $\mathbf{k} \cdot \mathbf{J} = \omega_\gamma \rho$, which leads to

$$|\mathbf{k}| L_{\ell\pm}^I(W, Q^2) = \omega_\gamma S_{\ell\pm}^I(W, Q^2). \quad (36)$$

Since the photon c.m. energy ω_γ vanishes for $Q^2 = Q_0^2 = W^2 - m^2$, the longitudinal multipole must have a zero at that momentum transfer, $L_{\ell\pm}^I(W, Q_0^2) = 0$. Furthermore, gauge invariance implies that the longitudinal and Coulomb multipoles take the same value in the real photon limit, $L_{\ell\pm}^I(W, Q^2 = 0) = S_{\ell\pm}^I(W, Q^2 = 0)$. Finally, the multipoles obey the following model-independent relations at physical threshold ($\mathbf{q} \rightarrow 0$) and pseudothreshold ($\mathbf{k} \rightarrow 0$):

$$\begin{aligned} (E_{\ell+}^I, L_{\ell+}^I) &\rightarrow k^\ell q^\ell \quad (\ell \geq 0) \\ (M_{\ell+}^I, M_{\ell-}^I) &\rightarrow k^\ell q^\ell \quad (\ell \geq 1) \\ (L_{\ell-}^I) &\rightarrow kq \quad (\ell = 1) \\ (E_{\ell-}^I, L_{\ell-}^I) &\rightarrow k^{\ell-2} q^\ell \quad (\ell \geq 2). \end{aligned} \quad (37)$$

According to Eq. (36) the Coulomb amplitudes acquire an additional factor k at pseudothreshold, i.e., $S_{\ell\pm}^I \sim k L_{\ell\pm}^I$. This limit is reached at $Q^2 = Q_{\text{pt}}^2 = -(W - m)^2$ (pseudothreshold), and because no direction is defined for $\mathbf{k} = 0$, the electric and longitudinal multipoles are no longer independent at this point,

$$E_{\ell+}^I/L_{\ell+}^I \rightarrow 1 \text{ and } E_{\ell-}^I/L_{\ell-}^I \rightarrow -\ell/(\ell-1) \text{ if } k \rightarrow 0. \quad (38)$$

In the case of the $N\Delta$ multipoles, Eq. (38) yields the following relation in the limit $\mathbf{k} \rightarrow 0$: $L_{1+}^{3/2} \rightarrow E_{1+}^{3/2} \rightarrow \mathcal{O}(k)$ and consequently $S_{1+}^{3/2} = k E_{1+}^{3/2}/\omega_\gamma \rightarrow \mathcal{O}(k^2)$. Although the pseudo-threshold is reached at the unphysical point $Q_{\text{pt}}^2 = -(M_\Delta - m)^2 \approx -0.084 \text{ GeV}^2$, it still influences the multipoles near $Q^2 = 0$ because of the relatively small excitation energy of the $\Delta(1232)$. In particular we get the

following relation for $Q^2 \rightarrow Q_{\text{pt}}^2$:

$$R_{SM} = \frac{S_{1+}^{(3/2)}}{M_{1+}^{(3/2)}} = \frac{k}{\omega_\gamma} \frac{E_{1+}^{(3/2)}}{M_{1+}^{(3/2)}} \rightarrow \frac{k}{M_\Delta - m} R_{EM}. \quad (39)$$

With increasing value of Q^2 , the Siegert relation fails to describe the experimental data. Moreover, it contains a singularity at $\omega_\gamma=0$, which occurs in $\Delta(1232)$ electroproduction already at $Q^2 = 0.64 \text{ GeV}^2$. However, we obtain a good overall description by using the idea of Ref. [59] that the ratio R_{SM} is related to the (elastic) form factors of the neutron,

$$R_{SM}(Q^2) = \frac{m k_\Delta(Q^2) G_E^n(Q^2)}{2 Q^2 G_M^n(Q^2)}. \quad (40)$$

This relation gives the necessary proportionality to the photon momentum at small Q^2 , describes the experimental value of the ratio over a wide range of Q^2 , and yields an asymptotic behavior consistent with the prediction of perturbative QCD that R_{SM} should approach a constant for $Q^2 \rightarrow \infty$. This leads to the following simple parametrization:

$$R_{SM}(Q^2) = -\frac{k_\Delta(Q^2)}{8m} \frac{a}{1+d\tau}, \quad (41)$$

with $\tau = Q^2/(4m^2)$, and the parameters a and d to be determined by a fit to the data. On the basis of this ansatz, the Coulomb coupling has been modified as follows:

$$\bar{A}_S^\Delta(W, Q^2) = A_S^0 \frac{1+\beta_S Q^2}{1+d\tau} \frac{k^2}{k_W k_W^\Delta} e^{-\gamma_S Q^2} G_D(Q^2), \quad (42)$$

with parameters given in Table 10. This leads to the multipole ratio

$$R_{SM}(Q^2) = \frac{A_S^0}{A_M^0} \frac{1}{1+d\tau} \left(\frac{1+\beta_S Q^2}{1+\beta_M Q^2} \right) \frac{k_\Delta}{k_W^\Delta}. \quad (43)$$

By construction this ratio vanishes in the Siegert limit, $Q^2 \rightarrow Q_{\text{pt}}^2$, and approaches a (negative) constant for $Q^2 \rightarrow \infty$ in agreement with perturbative QCD. However, a word of caution has to be added at this point. The polynomials and gaussians used to fit the data in the range of low and intermediate virtualities, $Q^2 < 10 \text{ GeV}^2$, should not be expected to yield realistic extrapolations to the higher values of Q^2 .

The correct Siegert limit is even more important for pion S -wave production in the threshold region, in which case the pseudo-threshold comes as close as $Q_{\text{pt}}^2 = -m_\pi^2 \approx -0.02 \text{ GeV}^2$. The term describing the pion cloud contribution has therefore been parameterized as follows:

$$L_{0+}^{\text{corr}}(W, Q^2) = \frac{\omega_\gamma}{\omega_{\text{pt}}} e^{-\beta(Q^2 - Q_{\text{pt}}^2)} E_{0+}^{\text{corr}}(W, Q^2), \quad (44)$$

where $\omega_{\text{pt}}^2 = -Q_{\text{pt}}^2 = (W - m)^2$. From a fit to π^0 electroproduction data near threshold [61], we obtain $\beta = 10 \text{ GeV}^{-2}$. In the future we intend to study pion

electroproduction near threshold in more detail.

Figures 17 and 18 display the super-global solutions of MAID2003 (dashed lines) and MAID2007 (solid lines) for the ratios R_{EM} and R_{SM} in comparison with other analyses. Different from our previous solution, the ratio R_{EM} of MAID2007 stays always below the zero line, in agreement with the original analysis of the data [13, 62] and also with the dynamical model of Sato and Lee [57] who concluded that R_{EM} remains negative and tends towards more negative values with increasing Q^2 . This indicates that the predicted helicity conservation at the quark level is irrelevant for the present experiments. We also analyzed the new data of Ref. [13] in the range of $3 \text{ GeV}^2 \leq Q^2 \leq 6 \text{ GeV}^2$ and found slightly decreasing values of R_{EM} from our single- Q^2 analysis. In this analysis we varied both the Δ and the Roper multipoles. For the ratio R_{SM} both the super-global and the single- Q^2 solutions yield ratios that asymptotically tend to a negative constant. This result is in good agreement with the prediction of Ref. [59] (dash-dotted curve in Fig. 18) but disagrees with our previous solution and with the analysis of Ref. [13]. As discussed before, the new solution has a large slope at small Q^2 as a consequence of the Siegert theorem. The following Fig. 19 displays the Q^2 dependence of the helicity amplitudes for the $N\Delta(1232)$ transition. Our single- Q^2 fit is in excellent agreement with the super-global solution, except for the values of $S_{1/2}$ at $Q^2 = 0.4$ and 0.525 GeV^2 .

5.4 Results for the higher resonances

Above the two-pion threshold we can no longer apply the two-channel unitarity and consequently the Watson theorem does not hold. Therefore, the background amplitude of the partial waves does not vanish at resonance as was the case for the $\Delta(1232)$ resonance. As an immediate consequence the resonance-background separation becomes more model-dependent. In MAID2007 we choose to separate the background and resonance contributions according to the K-matrix approximation. Furthermore, we recall that the absolute values of the helicity amplitudes are correlated with the values used for the total resonance width Γ_R and the single-pion branching ratio β_π . On the experimental side, the data at the higher energies are no longer as abundant as in the Δ region. However, the large data set recently obtained by the CLAS collaboration (see Table 9) enabled us to determine the transverse and longitudinal helicity couplings as functions of Q^2 for all the 4-star resonances below 1700 MeV. These data are available in the kinematical region of $1100 \text{ MeV} < W < 1680 \text{ MeV}$ and $0.4 \text{ GeV}^2 < Q^2 < 1.8 \text{ GeV}^2$.

The helicity amplitudes for the Roper resonance $P_{11}(1440)$ are shown in Fig. 20. Our latest super-global solution (solid lines) is in reasonable agreement with the single- Q^2 analysis. The figure shows a zero crossing of the transverse helicity amplitude at $Q^2 \approx 0.7 \text{ GeV}^2$ and a maximum at the relatively large momentum transfer

$Q^2 \approx 2.5 \text{ GeV}^2$. The longitudinal Roper excitation rises to large values around $Q^2 \approx 0.5 \text{ GeV}^2$ and in fact produces the strongest longitudinal amplitude we can find in our analysis. This answers the question raised by Li and Burkert [63] whether the Roper resonance is a radially excited 3-quark state or a quark-gluon hybrid, because in the latter case the longitudinal coupling should vanish completely. From the global fit we find the following parametrization for the Q^2 dependence of the Roper amplitudes for the proton and neutron channels:

$$A_{1/2}^p(Q^2) = A_{1/2}^{0,p}(1 - 1.22 Q^2 - 0.55 Q^8) e^{-1.51 Q^2},$$

$$S_{1/2}^p(Q^2) = S_{1/2}^{0,p}(1 + 40 Q^2 + 1.5 Q^8) e^{-1.75 Q^2}, \quad (45)$$

$$A_{1/2}^n(Q^2) = A_{1/2}^{0,n}(1 + 0.95 Q^2) e^{-1.77 Q^2},$$

$$S_{1/2}^n(Q^2) = S_{1/2}^{0,n}(1 + 2.98 Q^2) e^{-1.55 Q^2}, \quad (46)$$

where Q^2 should be inserted in units of GeV^2 . The numerical values of the helicity amplitudes for real photons are given in Table 11. At $Q^2=0$ the fit yields a large neutron value for the Coulomb amplitude $S_{1/2}^0$, but with increasing Q^2 the proton and neutron amplitudes become comparable.

Table 11. Helicity amplitudes for the $P_{11}(1440)$ resonance at $Q^2=0$ in units $10^{-3} \text{ GeV}^{-1/2}$.

	$A_{1/2}^0$		$S_{1/2}^0$	
	proton	neutron	proton	neutron
$P_{11}(1440)$	-61.4	54.1	4.2	-41.5

For all the higher resonances the transverse and longitudinal helicity amplitudes are simply parameterized by the form

$$A_\lambda(Q^2) = A_\lambda^0 (1 + \alpha Q^2) e^{-\beta Q^2}. \quad (47)$$

The values of the fit parameters A_λ^0 , α and β are listed in Tables 12 and 13. In the following Fig. 21 we present the results for the $S_{11}(1535)$. As is also known from η electroproduction, the transverse form factor falls off very slowly. At a virtuality of $Q^2 \approx 3 \text{ GeV}^2$ this resonance is much stronger than the $\Delta(1232)$ or the $D_{13}(1520)$ and only comparable to the Roper. However, due to its much smaller width as compared to the Roper, the S_{11} dominates over the Roper at large Q^2 . This result is in agreement with the inclusive electroproduction cross section on the proton, which clearly shows the dominance of the $\Delta(1232)$ at small momentum transfer whereas at the larger momentum transfers the second resonance region takes over.

In Fig. 22 we compare our results to those of Aznauryan *et al.* [64] who used a similar set of the CLAS data in the second resonance region. Our super-global solutions (solid lines) agree generally quite well with the

JLab-Yerevan analysis, which was performed with both an isobar model and dispersion analysis. The following

Table 12. The proton parameters for the higher resonances: α and β as defined by Eq. (47), in units GeV^{-2} , and $S_{1/2}^0$, the longitudinal amplitude at $Q^2 = 0$, in units $10^{-3} \text{ GeV}^{-1/2}$. The values for the transverse amplitudes $A_{1/2,3/2}^0$ are determined by the real photon physics and listed in Table 7.

proton	$A_{1/2}$		$A_{3/2}$		$S_{1/2}$		$S_{1/2}^0$
	α	β	α	β	α	β	
$D_{13}(1520)$	7.77	1.09	0.69	2.10	4.19	3.40	-63.6
$S_{11}(1535)$	1.61	0.70	—	—	23.9	0.81	-2.0
$S_{31}(1620)$	1.86	2.50	—	—	2.83	2.00	16.2
$S_{11}(1650)$	1.45	0.62	—	—	2.88	0.76	-3.5
$D_{15}(1675)$	0.10	2.00	0.10	2.00	0.00	0.00	0.00
$F_{15}(1680)$	3.98	1.20	1.00	2.22	3.14	1.68	-44.0
$D_{33}(1700)$	1.91	1.77	1.97	2.20	0.00	0.00	0.00
$P_{13}(1720)$	1.89	1.55	16.0	1.55	2.46	1.55	-53.0

Table 13. The neutron parameters for the higher resonances. The values for the transverse amplitudes $A_{1/2,3/2}^0$ are given in Table 8. Further notation as in Table 12.

neutron	$A_{1/2}$		$A_{3/2}$		$S_{1/2}$		$S_{1/2}^0$
	α	β	α	β	α	β	
$D_{13}(1520)$	-0.53	1.55	0.58	1.75	15.7	1.57	13.6
$S_{11}(1535)$	4.75	1.69	—	—	0.36	1.55	28.5
$S_{11}(1650)$	0.13	1.55	—	—	-0.50	1.55	10.1
$D_{15}(1675)$	0.01	2.00	0.01	2.00	0.00	0.00	0.00
$F_{15}(1680)$	0.00	1.20	4.09	1.75	0.00	0.00	0.00
$P_{13}(1720)$	12.7	1.55	4.99	1.55	0.00	0.00	0.00

Fig. 23 displays our super-global and single- Q^2 fits for the $D_{13}(1520)$ and $F_{15}(1680)$ resonances. The figure demonstrates that (I) the helicity non-conserving amplitude $A_{3/2}$ dominates for real photons and (II) with increasing values of Q^2 , $A_{3/2}$ drops faster than the helicity conserving amplitude $A_{1/2}$. As a consequence the asymmetry

$$A(Q^2) = \frac{|A_{1/2}|^2 - |A_{3/2}|^2}{|A_{1/2}|^2 + |A_{3/2}|^2} \quad (48)$$

changes rapidly from values close to -1 to values near $+1$ over a small Q^2 range. As is seen in Fig. 24, the asymmetry crosses the zero line at $Q^2 \approx 0.5 \text{ GeV}^2$ for the $D_{13}(1520)$ resonance and at $Q^2 \approx 0.8 \text{ GeV}^2$ for the $F_{15}(1680)$. As a comparison, the asymmetry A for the $\Delta(1232)$ resonance is practically constant over this Q^2 range with a value ≈ -0.5 . This again shows the special role of the Δ resonance, where the helicity conservation is not observed.

6 Conclusion

Using the world data base of pion photo- and electroproduction and recent data from Bates/MIT, ELSA/Bonn, MAMI/Mainz, and Jefferson Lab, we have extracted the longitudinal and transverse helicity amplitudes of nucleon resonance excitation for all the 4-star resonances below $W = 2$ GeV. For this purpose we have extended our unitary isobar model MAID and parameterized the Q^2 dependence of the transition amplitudes. The comparison between such super-global solutions with the corresponding single- Q^2 fits gives us confidence in the obtained helicity couplings for the $P_{33}(1232)$, $P_{11}(1440)$, $S_{11}(1535)$, $D_{13}(1520)$, and $F_{15}(1680)$ resonances, even though the model uncertainty is still quite large, particularly for the longitudinal amplitudes.

For the higher 4-star and all 3-star resonances the situation is less clear. This deplorable situation reflects the fact that a model-independent analysis requires precision data over a large kinematical range. In some cases double-polarization experiments will be helpful, as has already been shown for pion photoproduction. Furthermore, charged pion electroproduction data are needed with the same quantity and quality as for neutral pions, in order to resolve the ambiguities in the isospin structure, in particular for the S_{11} and S_{31} resonances. While we have mostly discussed the electroproduction from proton targets, also the existing neutron data have been analyzed. The latter are of course less abundant, and moreover no new neutron data have been reported over the recent years. Because the isospin symmetry is most likely on safe grounds in the resonance region, only the electromagnetic neutron couplings with isospin $1/2$ are still lacking. In spite of the discussed problems, we have implemented a super-global solution also for the neutron amplitudes in MAID07.

Pion photo- and electroproduction are invaluable tools to study the resonance structure of the nucleon. With the advent of the new c.w. electron accelerators, new precision experiments have afforded a host of new data to unravel this structure in the first and second resonance regions. In particular, electroproduction has provided new insights in the spatial distribution of the nucleon-resonance transition densities. However, in order to get the whole picture, several challenges remain:

- Dedicated experiments to investigate the higher energy region, which have to include an intense study of the polarization degrees of freedom. Experience has shown that even the physics of the $\Delta(1232)$ requires a full-fledged program to measure the spin observables in order to understand the background of the non-resonating multipoles.
- A fresh approach to also determine the excitation spectrum of the neutron. As an example, the comparison of the Roper or $P_{11}(1440)$ helicity amplitudes for proton and neutron will shed light on the structure of this enigmatic resonance.

- The open question of the excitation spectrum in the third resonance region and above deserves further studies in both theory and experiment. This includes “missing” and “exotic”, e.g., 5-quark resonances as well as more mundane second and third resonances in a multipole, which show up in a particular analysis and not in another one.

In conclusion we hope that MAID2007, just as other approaches based on partial-wave analysis, dynamic models, coupled-channels calculations, and dispersion theory, will contribute to settle the mentioned issues and thus to improve our still somewhat vestigial knowledge of the nucleon’s resonance structure.

Acknowledgment

This work was supported by the Deutsche Forschungsgemeinschaft through the SFB 443, by the joint project NSC/DFG 446 TAI113/10/0-3 and by the joint Russian-German Heisenberg-Landau program.

References

1. G. Höhler *et al.*, *Handbook of Pion-Nucleon Scattering*, Physics Data 12-1 (Karlsruhe, 1979).
2. W.-M. Yao *et al.* [Particle Data Group], J. Phys. G **33**, 1 (2006).
3. For an overview and further references see S. Boffi, C. Giusti, F.D. Pacati, and M. Radici, *Electromagnetic Response of Atomic Nuclei*, Clarendon Press, Oxford (1996) p. 114 pp.
4. R. Beck *et al.*, Phys. Rev. Lett. **78**, 606 (1997).
5. J.J. Kelly *et al.*, Phys. Rev. Lett. **95**, 102001 (2005) and Phys. Rev. C **75**, 025201 (2007).
6. D. Drechsel, O. Hanstein, S.S. Kamalov, and L. Tiator, Nucl. Phys. A **645**, 145 (1999); <http://www.kph.uni-mainz.de/MAID/>.
7. R.A. Arndt, I.I. Strakovsky, and R.L. Workman, Phys. Rev. C **53**, 430 (1996) (SP97 solution of the VPI analysis).
8. V. Burkert, Proc. of Topical Workshop on “Excited Baryons 1988”, Troy, New York (1988), eds. G. Adams, N. Mukhopadhyay, and P. Stoler, World Scientific, Singapore (1989) p. 122.
9. S.S. Kamalov, D. Drechsel, L. Tiator, and S.N. Yang, Proc. of Workshop on “The Physics of Excited Nucleons”, Mainz, Germany (2001), eds. D. Drechsel and L. Tiator, P. World Scientific, Singapore (2001), p. 197.
10. S.S. Kamalov, S.N. Yang, D. Drechsel, O. Hanstein, L. Tiator, Phys. Rev. C **64**, 032201 (2001); <http://www.kph.uni-mainz.de/MAID/DMT/>.
11. J.J. Kelly, Phys. Rev. C **70**, 068202 (2004).
12. L. Tiator and S.S. Kamalov, Proc. of Workshop on “The Physics of Excited Nucleons”, Tallahassee, FL, USA (2005), eds. S. Capstick, V. Crede and P. Eugenio, World Scientific, Singapore (2006), p. 16.
13. M. Ungaro *et al.*, Phys. Rev. Lett. C **90**, 112003 (2006).
14. S.N. Yang, J. Phys. G **11**, L205 (1985).
15. S.S. Kamalov, and S.N. Yang, Phys. Rev. Lett. **83**, 4494 (1999).
16. R.A. Arndt, I.I. Strakovsky, and R.L. Workman, Phys. Rev. C **53**, 430 (1996) (SP99 solution of the GWI/SAID analysis).

17. S.S. Kamalov, G.Y. Chen, S.N. Yang, D. Drechsel, and L. Tiator, Phys. Lett. B **522**, 27 (2001).
18. J.M. Laget, Phys. Rep. **69**, 1 (1981).
19. V. Bernard, N. Kaiser, and Ulf-G. Meißner, Phys. Lett. B **268**, 291 (1991); Z. Phys. C **70**, 483 (1996).
20. R. Leukel, PhD thesis, Mainz (2001), <http://wwwa2.kph.uni-mainz.de/A2/>.
21. J. Ahrens *et al.*, Phys. Rev. Lett. **87**, 022003 (2001) and **88**, 232002 (2002).
22. I. Preobrajenski, PhD thesis, Mainz (2001), <http://wwwa2.kph.uni-mainz.de/A2/>.
23. J. Ahrens, *et al.*, Phys. Rev. C **87**, 045204 (2006).
24. O. Bartalini *et al.*, Phys. Lett. B **554**, 113 (2002).
25. O. Bartalini *et al.*, Eur. Phys. J. A **26**, 399 (2005).
26. A. Shafi *et al.* Phys. Rev. C **70**, 035204 (2004).
27. O. Bartholomy *et al.*, Phys. Rev. Lett. **94**, 012003 (2005).
28. R.A. Arndt, W.J. Briscoe, I.I. Strakovsky, and R.L. Workman, Phys. Rev. C **66**, 055213 (2002); <http://gwdac.phys.gwu.edu/>.
29. M. Dugger *et al.* Phys. Rev. C **76**, 025211 (2007)
30. J.C. Bergstrom *et al.*, Phys. Rev. C **53**, R1052 (1996) and **55**, 2016 (1997).
31. A. Schmidt *et al.*, Phys. Rev. Lett. **87**, 232501 (2001).
32. O. Hanstein, D. Drechsel, and L. Tiator, Phys. Lett. B **385**, 45 (1996) and Nucl. Phys. A **632**, 561 (1998).
33. S.S. Kamalov, L. Tiator, D. Drechsel, R.A. Arndt, C. Bennhold, I.I. Strakovsky, and R.L. Workman, Phys. Rev. C **66**, 065206 (2002).
34. I.G. Aznauryan, Phys. Rev. C **67**, 015209 (2003).
35. G.Y. Chen, S. Kamalov, S.N. Yang, D. Drechsel, and L. Tiator, Nucl. Phys. A **723**, 447 (2003).
36. D. Drechsel and L. Tiator, J. Phys. G: Nucl. Phys. **18**, 449 (1992).
37. L.H. Hand, Phys. Rev. **129**, 1834 (1963).
38. F.J. Gilman, Phys. Rev. **167**, 1365 (1968).
39. G.F. Chew, M.L. Goldberger, F.E. Low, and Y. Nambu, Phys. Rev. **106**, 1345 (1957).
40. G. Knöchlein, D. Drechsel, and L. Tiator, Z. Phys. A **352**, 327 (1995).
41. R.A. Arndt, W.J. Briscoe, I.I. Strakovsky, and R.L. Workman, <http://gwdac.phys.gwu.edu/>.
42. T. Bantes and R. Gothe, private communication.
43. K. Joo *et al.*, Phys. Rev. Lett. **88**, 122001-1 (2002).
44. K. Joo *et al.*, Phys. Rev. C **68**, 032201 (2003).
45. K. Joo *et al.*, Phys. Rev. C **70**, 042201 (2004).
46. H. Egiyan *et al.*, Phys. Rev. C **73**, 025204 (2006).
47. C. Mertz *et al.*, Phys. Rev. Lett. **86**, 2963 (2001).
48. S. Stave *et al.*, Eur. Phys. J. A **30**, 471 (2006).
49. Th. Pospischil *et al.*, Phys. Rev. Lett. **86**, 2959 (2001).
50. D. Elsner *et al.*, Eur. Phys. J. A **27**, 91 (2006).
51. G. Laveissiere *et al.*, Phys. Rev. C **69**, 045202 (2004).
52. W.W. Ash *et al.*, Phys. Lett. B **24**, 165 (1967).
53. H.F. Jones and M.D. Scadron, Annals Phys. **81**, 1 (1973).
54. L. Tiator, D. Drechsel, S.S. Kamalov, and S.N. Yang, Eur. Phys. J. A **17**, 357 (2003).
55. G.C. Gellas, T.R. Hemmert, C.N. Ktorides, and G.I. Poulis, Phys. Rev. D **60**, 054022 (1999); T.A. Gail and T.R. Hemmert, Eur. Phys. J. A **28**, 91 (2006).
56. V. Pascalutsa and M. Vanderhaeghen, Phys. Rev. Lett. **95**, 232001 (2005) and Phys. Rev. D **73**, 034003 (2005).
57. T. Sato and T.S.H. Lee, Phys. Rev. C **63**, 055201 (2001).
58. D. Drechsel and L. Tiator, AIP Conf. Proc. **904** 129 (2007).
59. A.J. Buchmann, Phys. Rev. Lett. **93**, 212301-1 (2004).
60. R.A. Arndt, R.L. Workman, Z. Li and L.D. Roper, Phys. Rev. C **42**, 1864 (1990).
61. M. Weis *et al.* (A1 Collaboration), arXiv:0705.3816 [nucl-ex].
62. V.V. Frolov *et al.*, Phys. Rev. Lett. **82**, 45 (1999).
63. Z. Li, V. Burkert, and Z. Li, Phys. Rev. D **46**, 70 (1992).
64. I. Aznauryan, V. Burkert, H. Egiyan, K. Joo, R. Minehart and L.C. Smith, Phys. Rev. C **71**, 015201 (2005).

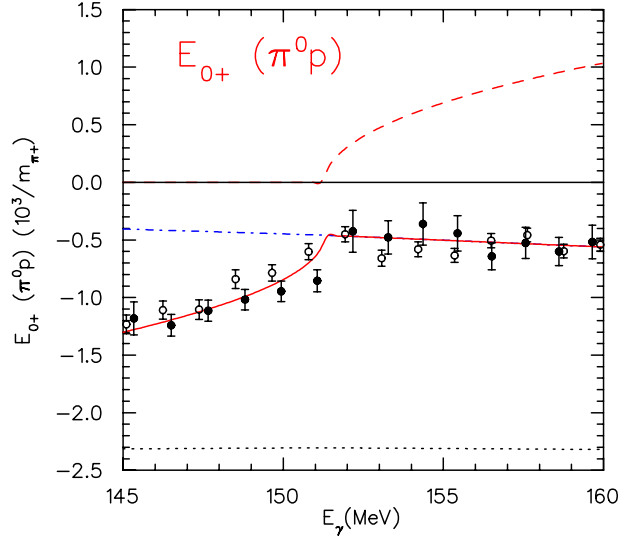


Fig. 1. The E_{0+} multipole for $\gamma p \rightarrow \pi^0 p$. Real part: the results of MAID98 (dotted line) and MAID2007 without the cusp effect (dashed-dotted line) as well as the full MAID2007 calculation (red solid line). The red dashed line is the imaginary part of the full MAID2007 solution. The data points are from Refs. [30](\bullet) and [31](\circ).

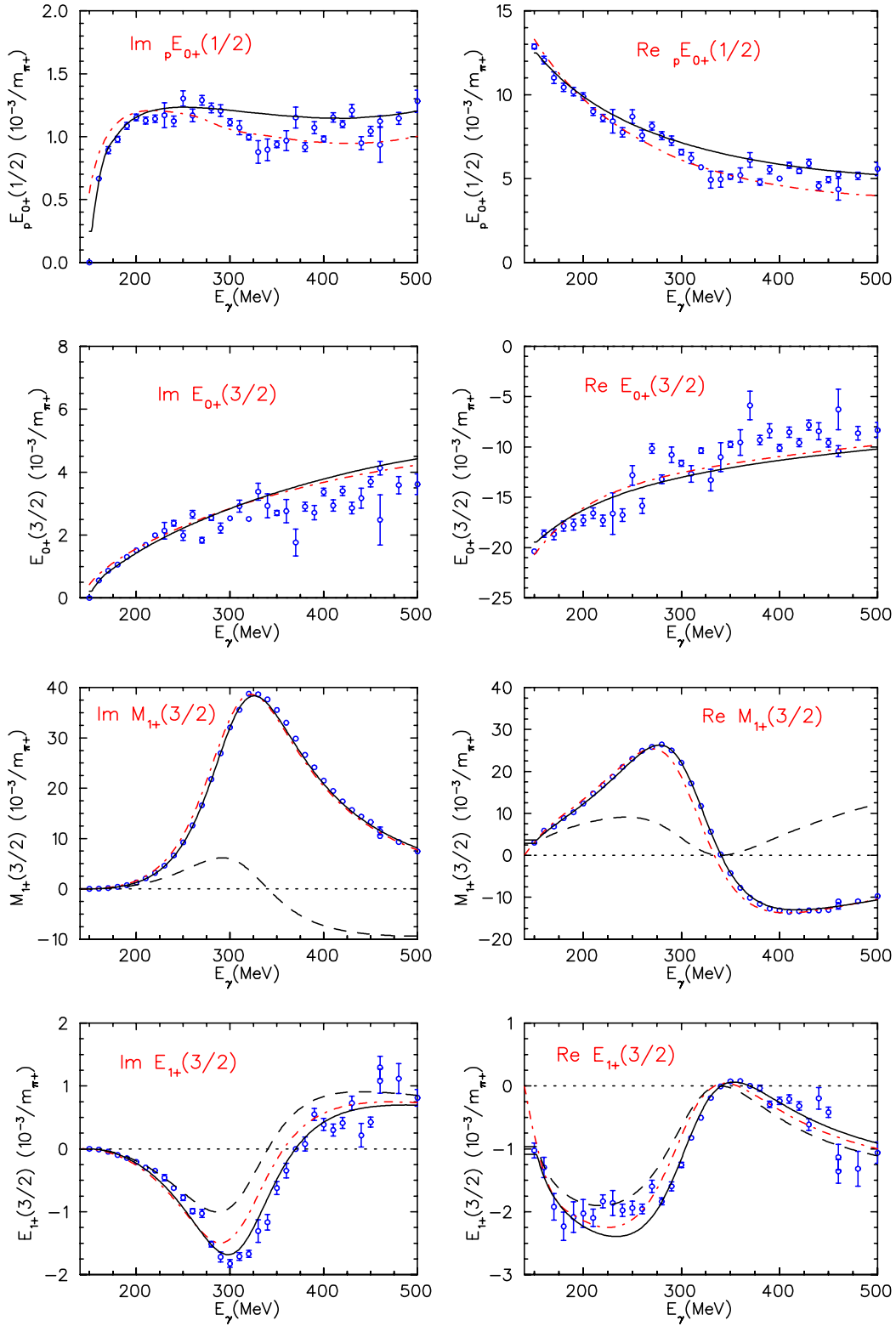


Fig. 2. The global solutions of MAID2007 (solid lines) and GWU/SAID [29] (red dashed-dotted lines, solution FA06K) for the multipoles $pE_{0+}^{1/2}$, $E_{0+}^{3/2}$, $M_{1+}^{3/2}$, and $E_{1+}^{3/2}$ as function of the photon lab energy E_γ in the first resonance region. The blue open circles show our single-energy solution. The dashed lines represent our unitarized background contributions in the $M_{1+}^{3/2}$ and $E_{1+}^{3/2}$ multipoles.

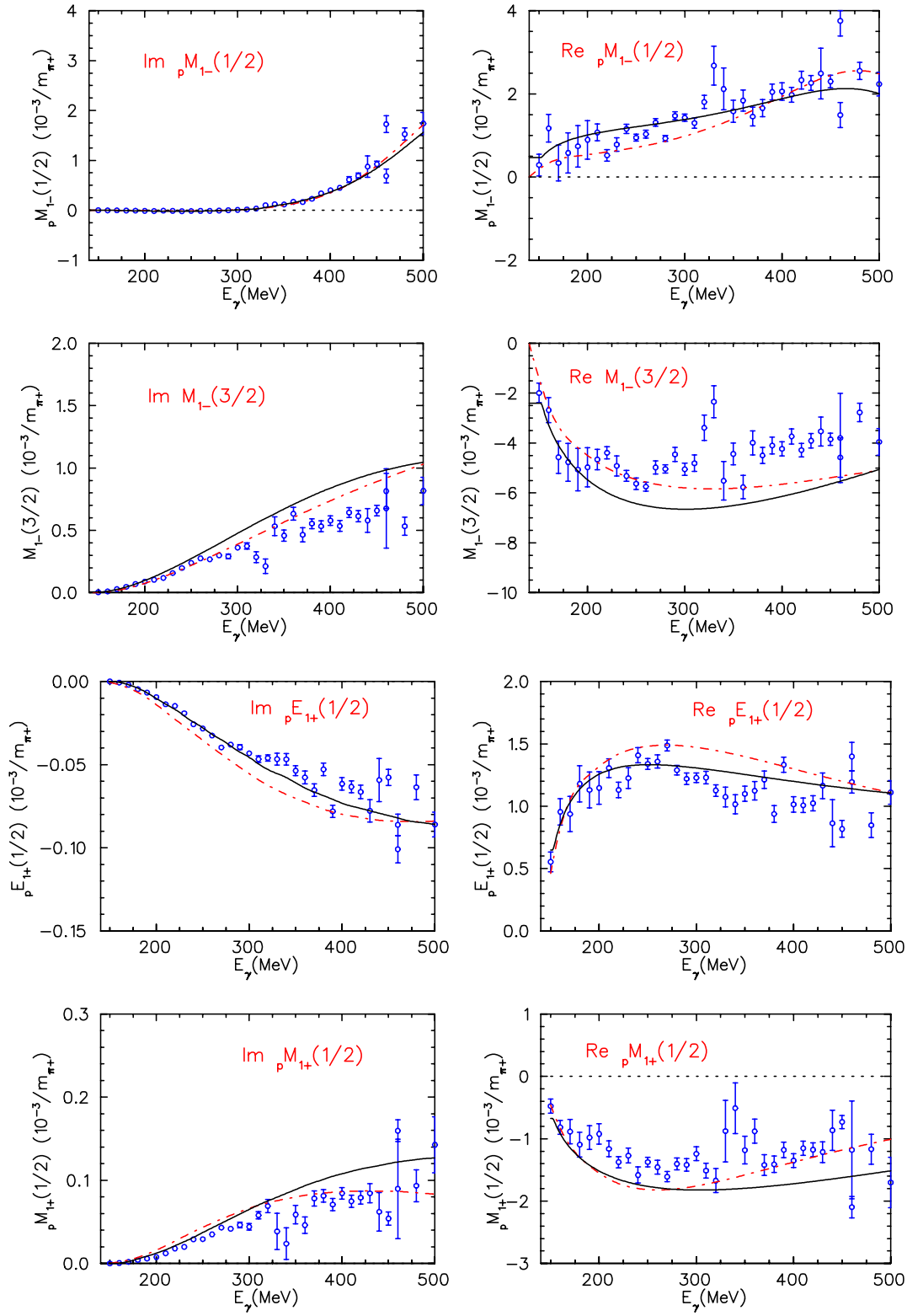


Fig. 3. The multipoles ${}_pM_{1-}^{1/2}$, $M_{1-}^{3/2}$, ${}_pE_{1+}^{1/2}$, and ${}_pM_{1+}^{1/2}$ as function of the photon lab energy E_γ . Further notation as in Fig. 2.

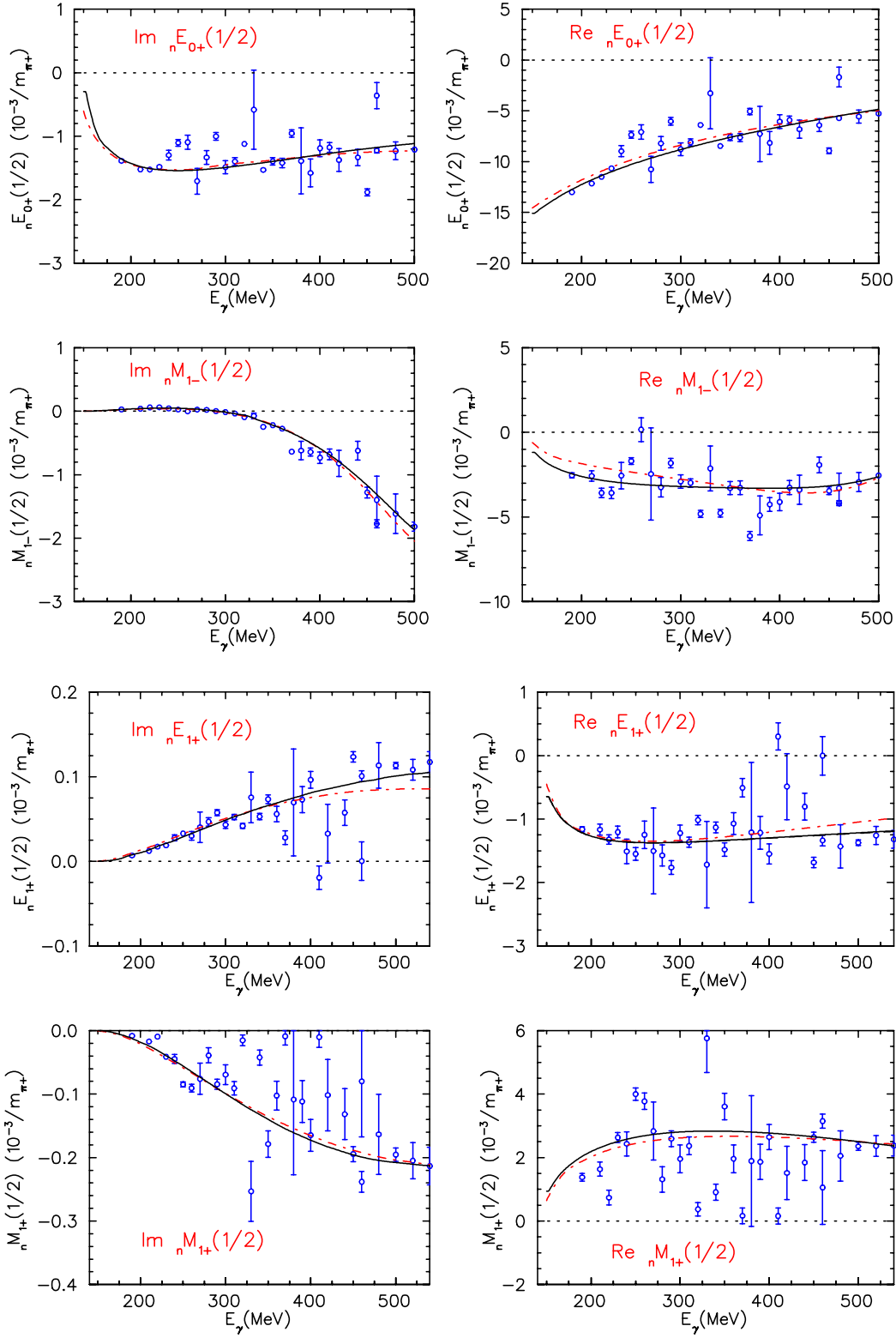


Fig. 4. The multipoles ${}_n E_{0+}^{1/2}$, ${}_n M_{1-}^{1/2}$, ${}_n E_{1+}^{1/2}$, and ${}_n M_{1+}^{1/2}$ as function of the photon lab energy E_γ . Further notation as in Fig. 2.

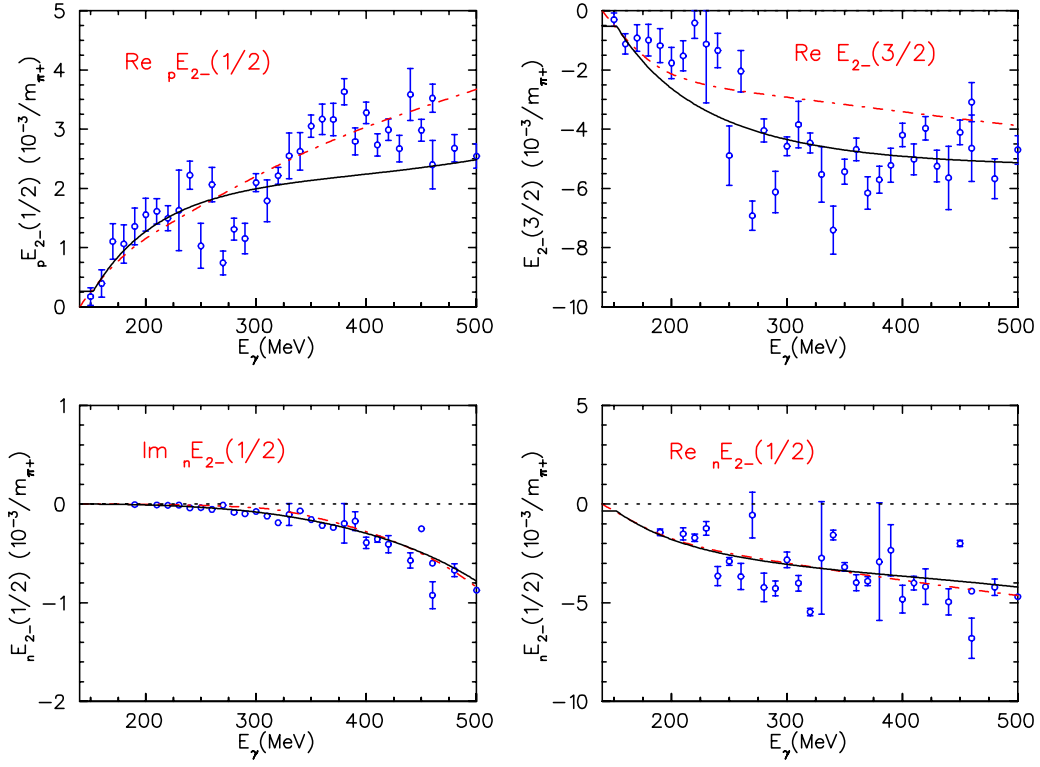


Fig. 5. The multipoles $pE_{2-}^{1/2}$, $E_{2-}^{3/2}$, and $nE_{2-}^{1/2}$ as function of the photon lab energy E_γ . Further notation as in Fig. 2.

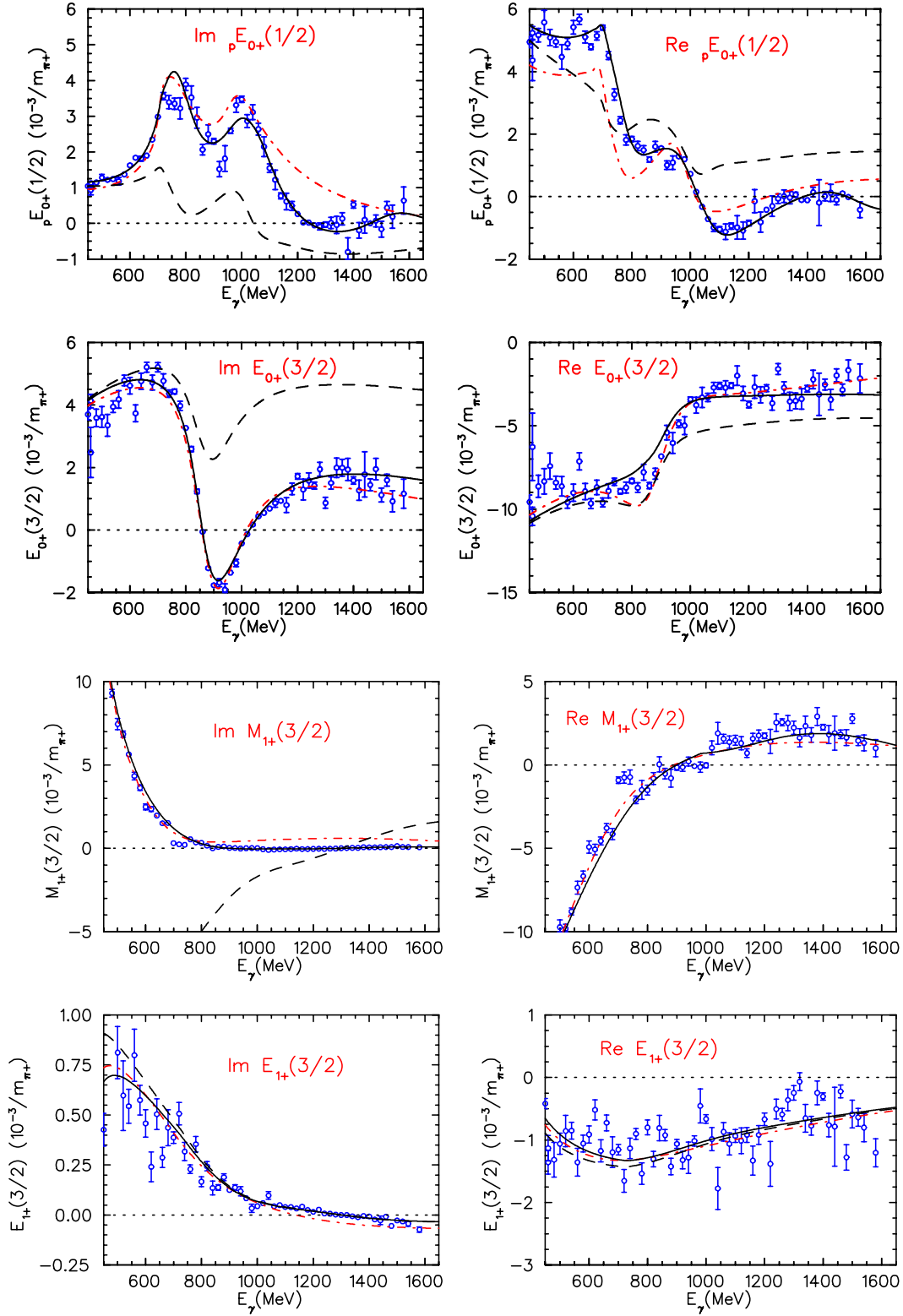


Fig. 6. The global solutions of MAID2007 (solid lines) and GWU/SAID [29] (red dashed-dotted lines, solution FA06K) for the multipoles ${}_pE_{0+}^{1/2}$, $E_{0+}^{3/2}$, $M_{1+}^{3/2}$, and $E_{1+}^{3/2}$ as function of the photon lab energy E_γ in the second and third resonance regions. The blue open circles show our single-energy solution. The dashed lines represent our unitarized background given by Eq. (15). Note that the background for $\text{Re } M_{1+}^{3/2}$ is out of scale.

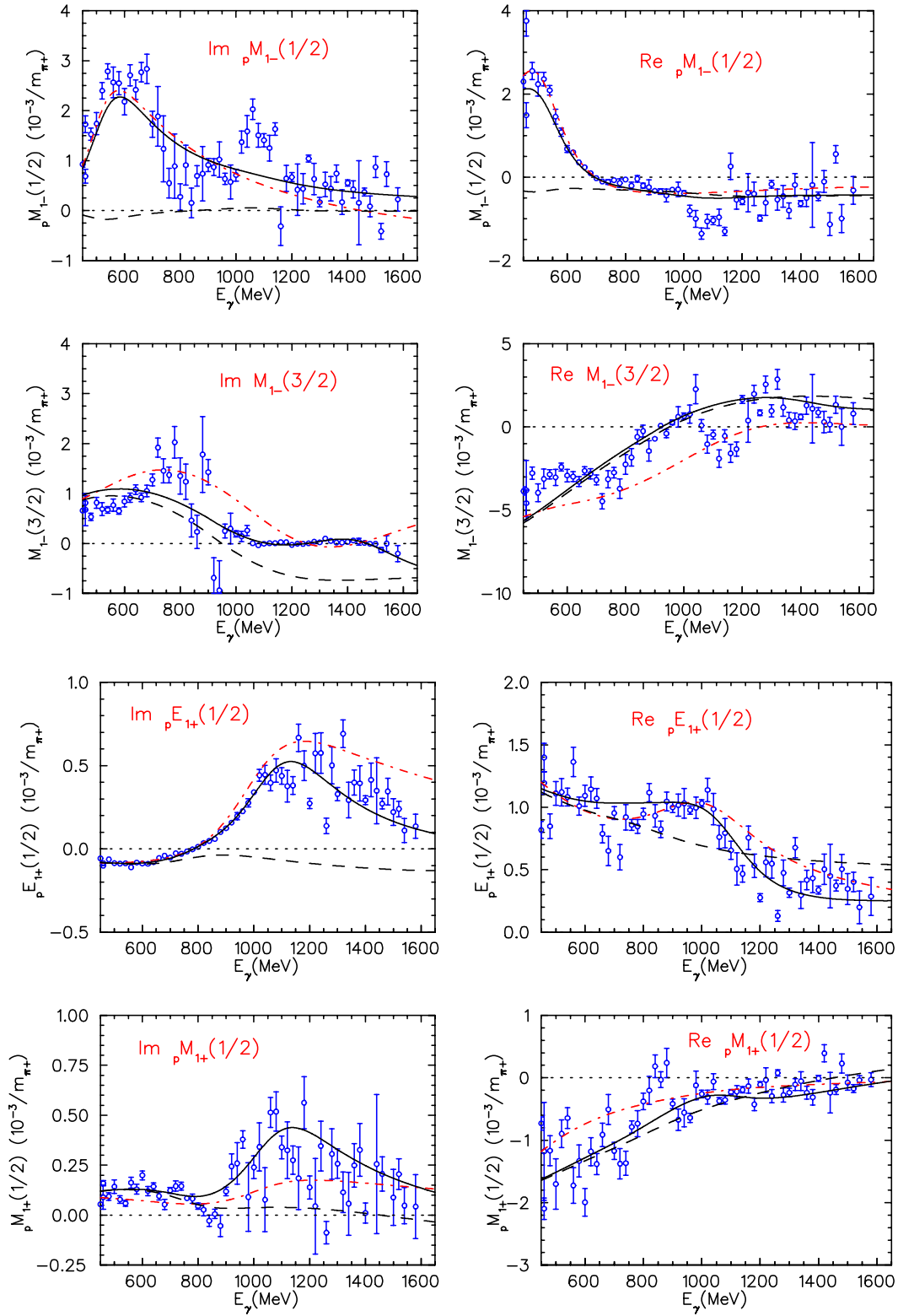


Fig. 7. The global solutions of MAID2007 (black solid lines) and GWU/SAID [29] (red dashed-dotted lines) for the multipoles $pM_{1-}^{1/2}$, $M_{1-}^{3/2}$, $pE_{1+}^{1/2}$, and $pM_{1+}^{1/2}$ as function of the photon lab energy E_γ in the second and third resonance regions. Further notation as in Fig. 6.

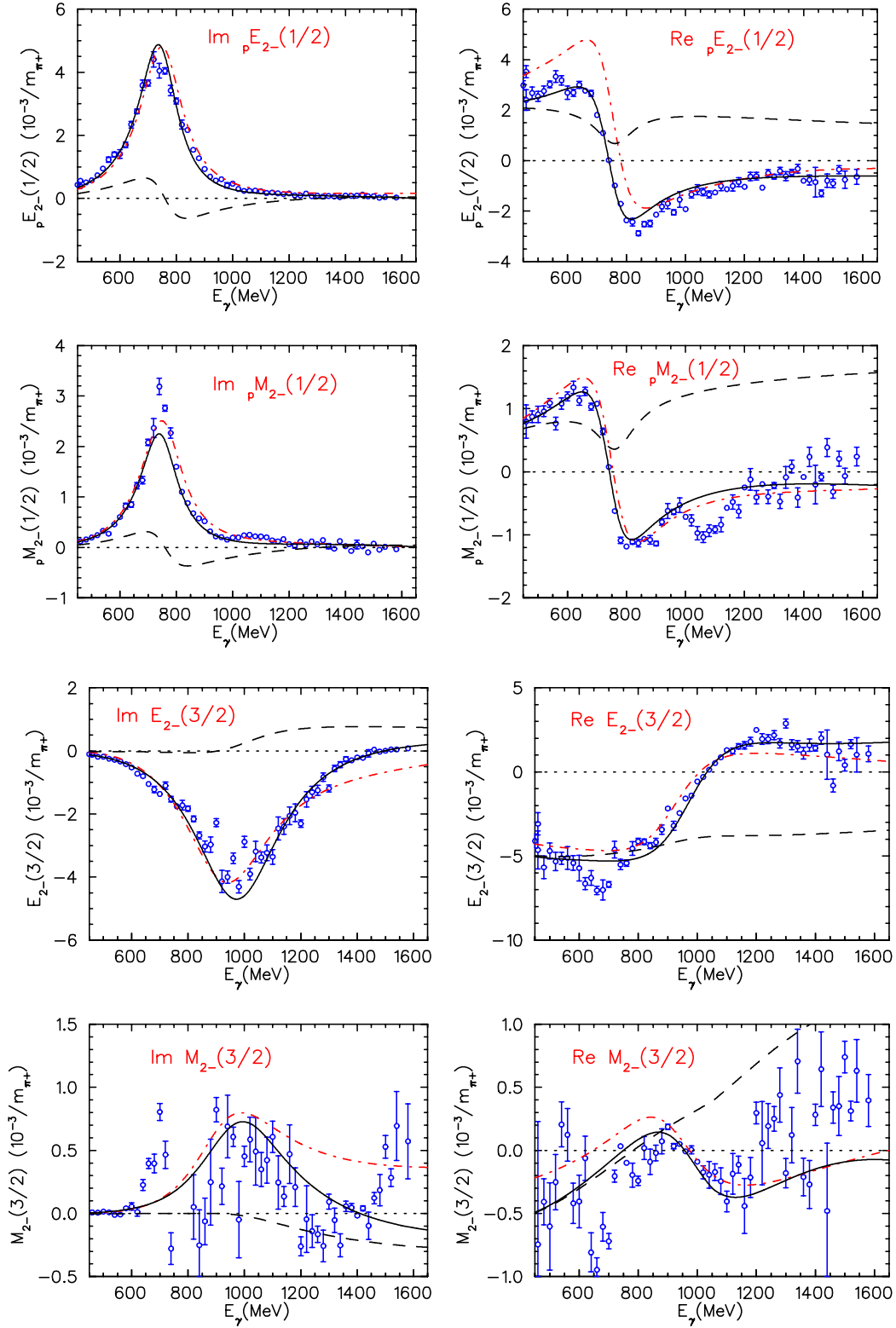


Fig. 8. The global solutions of MAID2007 (black solid lines) and GWU/SAID [29] (red dashed-dotted lines) for the multipoles $pE_{2-}^{1/2}$, $pM_{2-}^{1/2}$, $E_{2-}^{3/2}$, and $M_{2-}^{3/2}$ as function of the photon lab energy E_γ in the second and third resonance regions. Further notation as in Fig. 6.

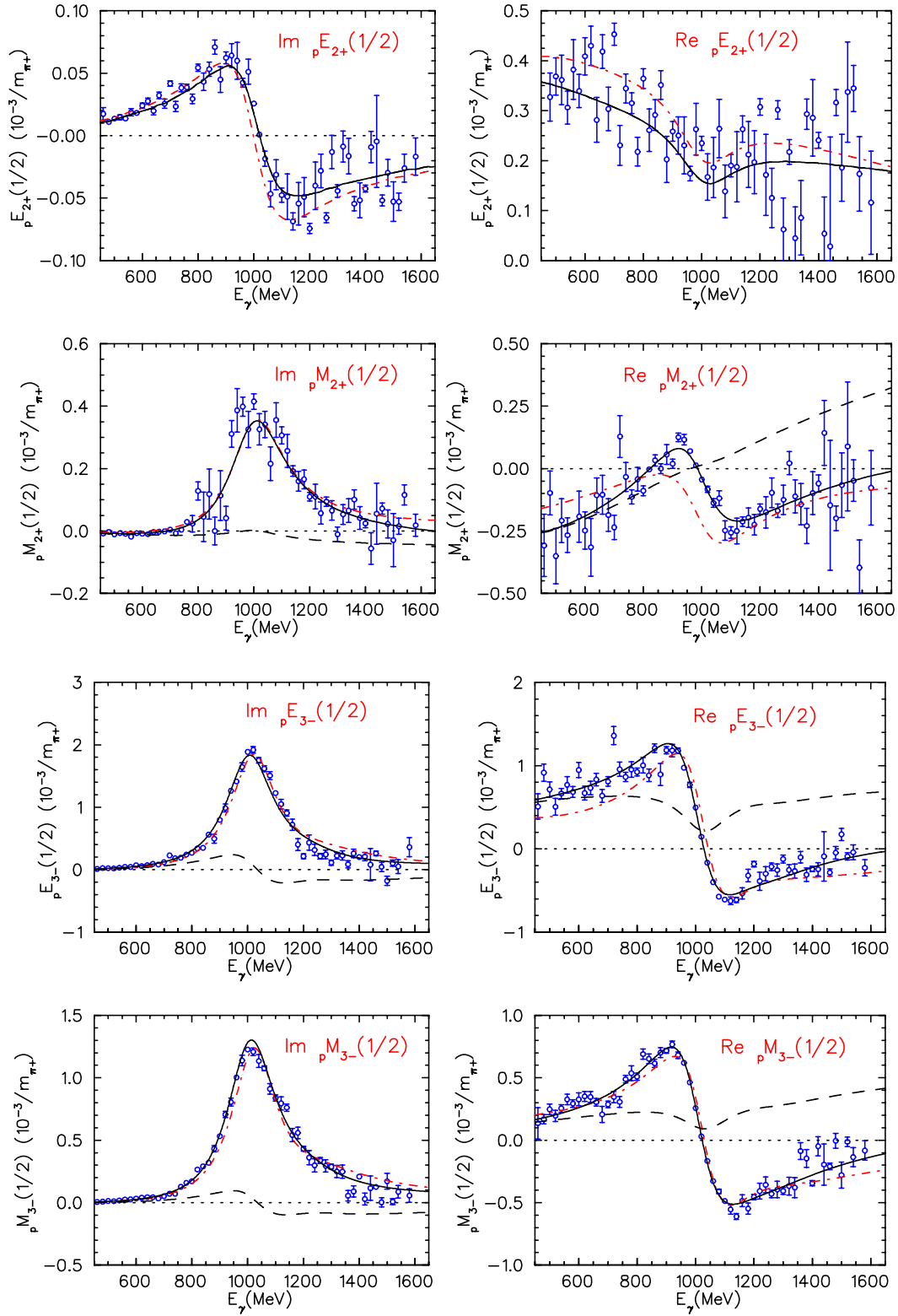


Fig. 9. The global solutions of MAID2007 (solid lines) and GWU/SAID [29] (red dashed-dotted lines) for the multipoles $pE_{2+}^{1/2}$, $pM_{2+}^{1/2}$, $pE_{3-}^{1/2}$, and $pM_{3-}^{1/2}$ as function of the photon lab energy E_γ in the second and third resonance regions. Further notation as in Fig. 6. The resonance contribution to the $pE_{2+}^{1/2}$ multipole is very small, and therefore the solid and dashed lines coincide.

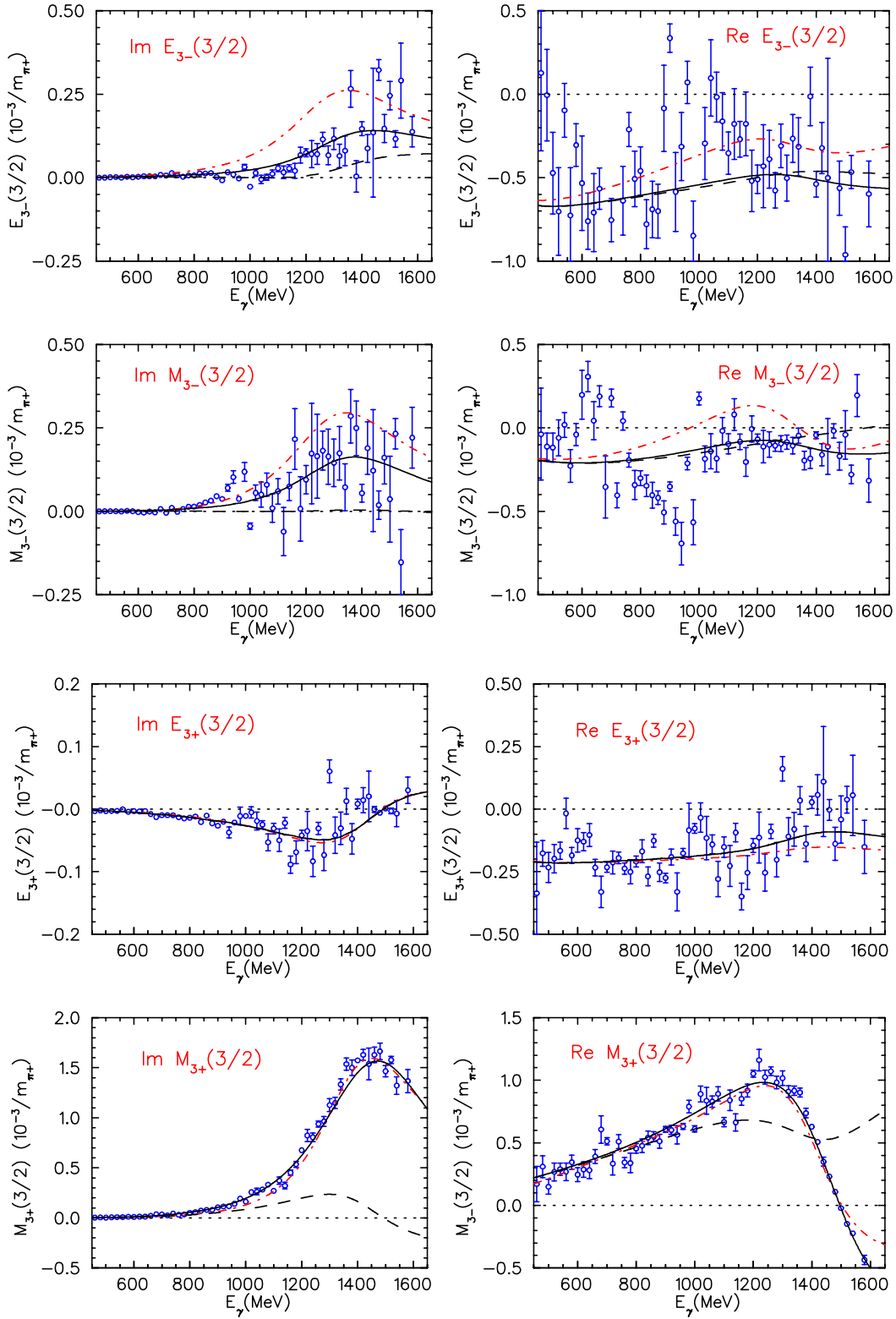


Fig. 10. The global solutions of MAID2007 (solid lines) and GWU/SAID [29] (red dashed-dotted lines) for the multipoles $E_{3-}^{3/2}$, $M_{3-}^{3/2}$, $E_{3+}^{3/2}$, and $M_{3+}^{3/2}$ as function of the photon lab energy E_γ in the second and third resonance regions. Further notation as in Fig. 6. The resonance contribution to the $E_{3+}^{3/2}$ multipole is very small, and therefore the solid and dashed lines coincide.

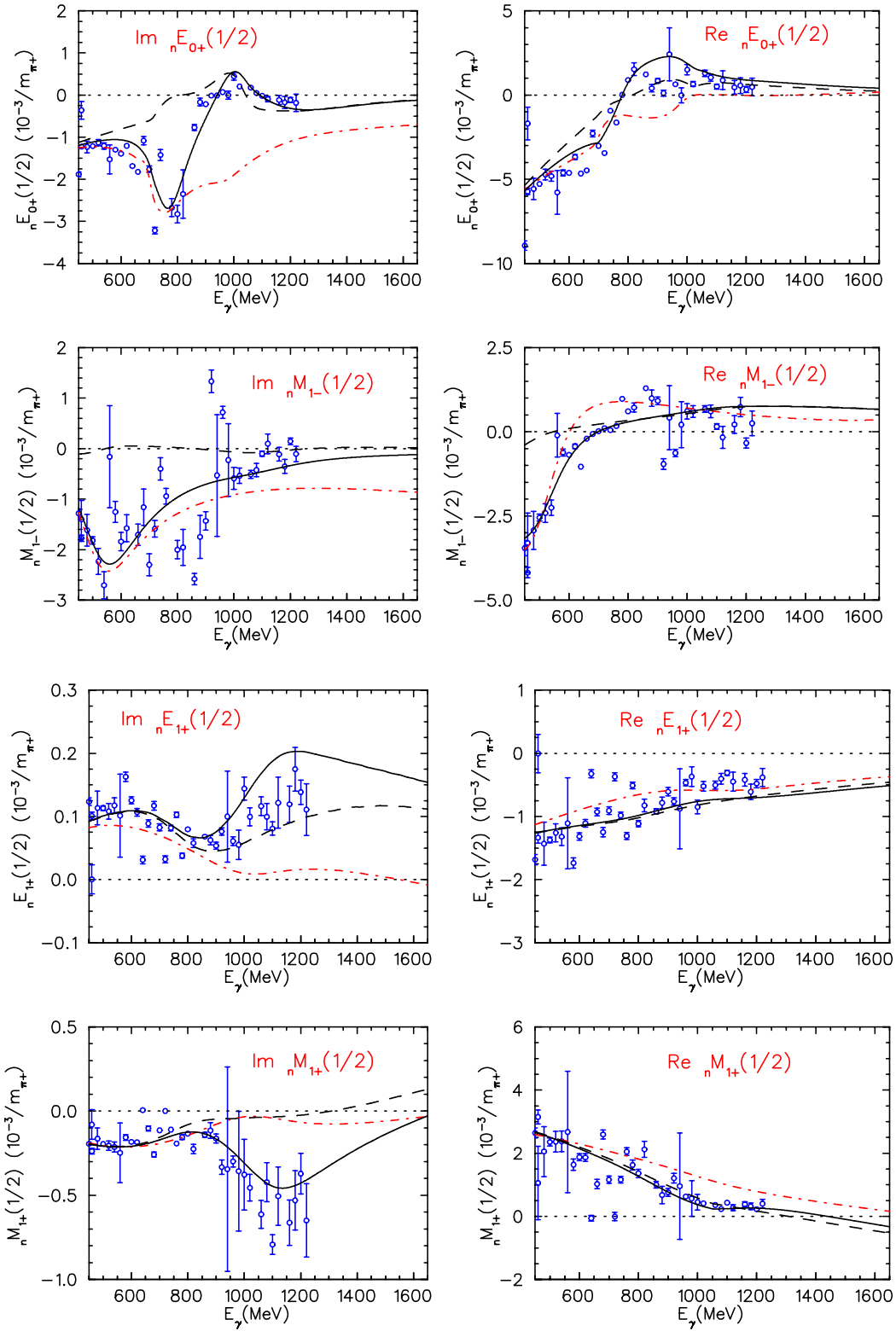


Fig. 11. The global solutions of MAID2007 (solid lines) and GWU/SAID [29] (red dashed-dotted lines) for the multipoles $nE_{0+}^{1/2}$, $nM_{1-}^{1/2}$, $nE_{1+}^{1/2}$, and $nM_{1+}^{1/2}$ as function of the photon lab energy E_γ in the second and third resonance regions. Further notation as in Fig. 6.

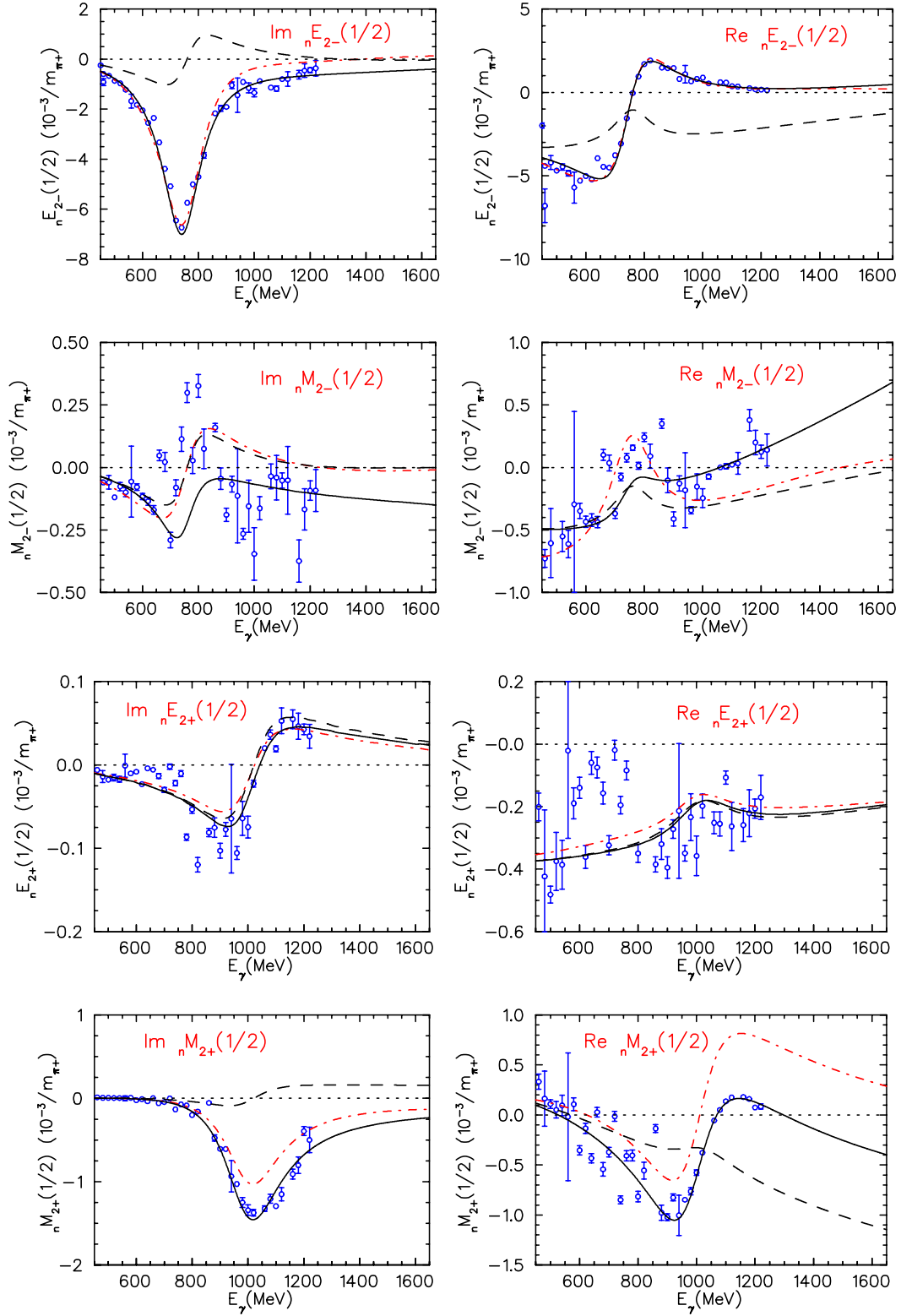


Fig. 12. The global solutions of MAID2007 (solid lines) and GWU/SAID [29] (red dashed-dotted lines) for the multipoles $nE_{2-}^{1/2}$, $nM_{2-}^{1/2}$, $nE_{2+}^{1/2}$, and $nM_{2+}^{1/2}$ as function of the photon lab energy E_γ in the second and third resonance regions. Further notation as in Fig. 6.

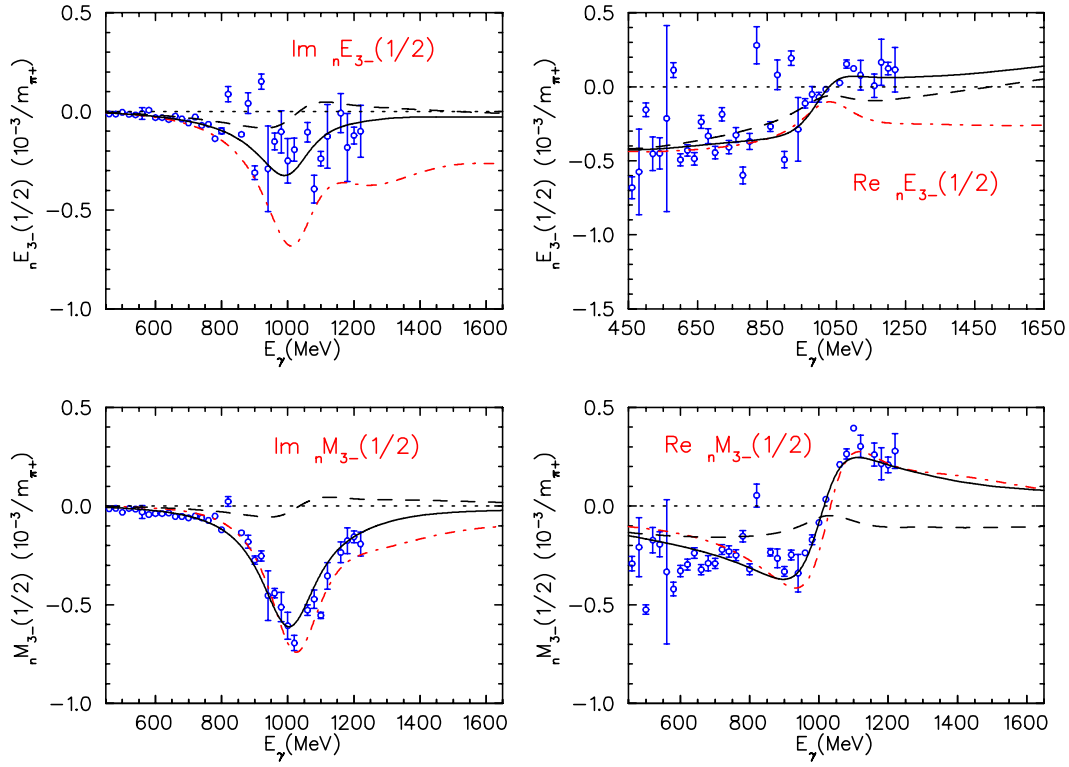


Fig. 13. The global solutions of MAID2007 (solid lines) and GWU/SAID [29] (red dashed-dotted lines) for the multipoles ${}_nE_{3-}^{1/2}$ and ${}_nM_{3-}^{1/2}$ as function of the photon lab energy E_γ in the second and third resonance regions. Further notation as in Fig. 6.

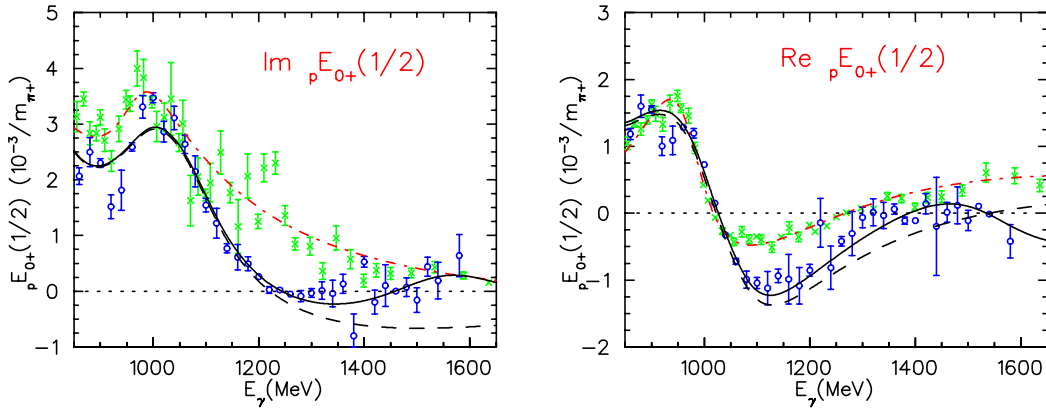


Fig. 14. The contribution of a third S_{11} resonance in the ${}_pE_{0+}^{1/2}$ multipole with $M_R=1950$ MeV, $\Gamma_R=200$ MeV, single-pion branching ratio $\beta_\pi=0.4$, and helicity amplitude $A_{1/2}=0.028$ GeV $^{-1/2}$. The solid and dashed lines are our global solutions with and without this resonance, respectively. The red dashed-dotted lines represent the global SAID solution. The blue open circles and green crosses are the single-energy solutions of MAID2007 and the SAID, respectively. This resonance is included in MAID2007.

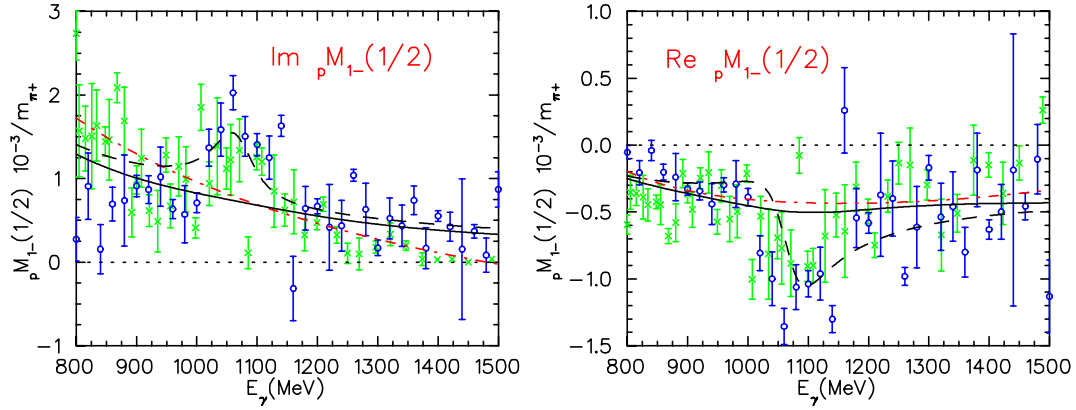


Fig. 15. The contribution of a second P_{11} resonance in the $pM_{1-}^{1/2}$ multipole with $M_R=1700$ MeV, $\Gamma_{tot}=47$ MeV, single-pion branching ratio $\beta_\pi=0.1$, and helicity amplitude $A_{1/2} = -0.024$ $\text{GeV}^{-1/2}$. The solid and dashed lines are our global solutions without and with this resonance, respectively. Further notation as in Fig. 14. The $P_{11}(1700)$ is *not* included in MAID2007.

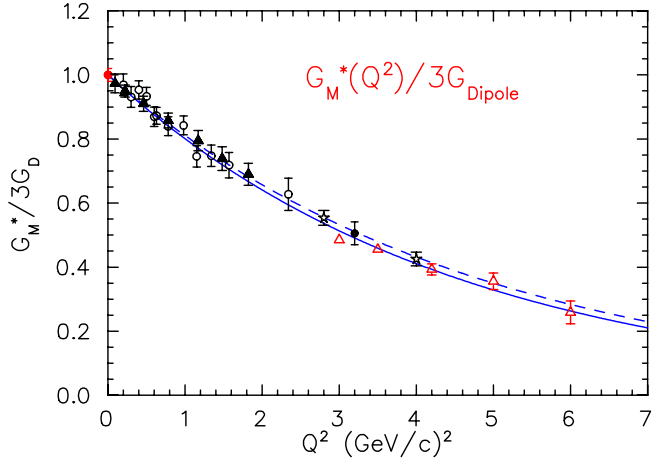


Fig. 16. The Q^2 dependence of the magnetic form factor G_M^* for the $N\Delta(1232)$ transition divided by $3G_D(Q^2)$. The solid and dashed blue lines are the results of MAID2007 and MAID2003, respectively. The red open triangles represent the new JLab data of Ungaro *et al.* [13]. See Ref. [10] for the notation of the other data points.

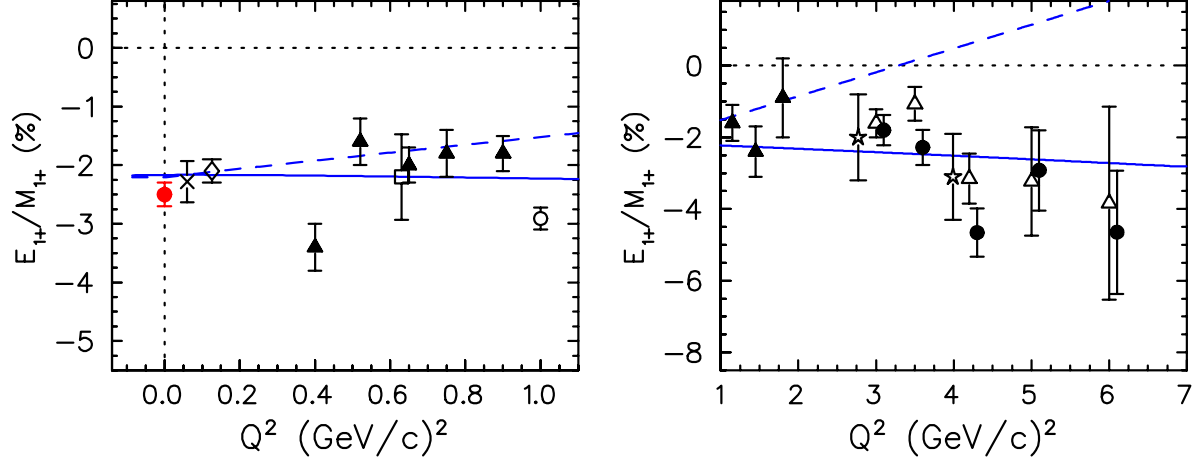


Fig. 17. The Q^2 dependence of the ratio R_{EM} at the $\Delta(1232)$ resonance. The blue solid and dashed lines are the super-global solutions from MAID2007 and MAID2003, respectively. The data points are from Refs. [42] (open square), [43] (solid triangles), [47] (open diamond), [48] (cross), [5] (open circle), [62] (asterisks), and [13] (open triangles). The green solid circle at $Q^2 = 0$ in the left panel is from Ref. [4], and the black solid circles in the right panel are obtained by our single- Q^2 analysis of the data from Ref. [13].

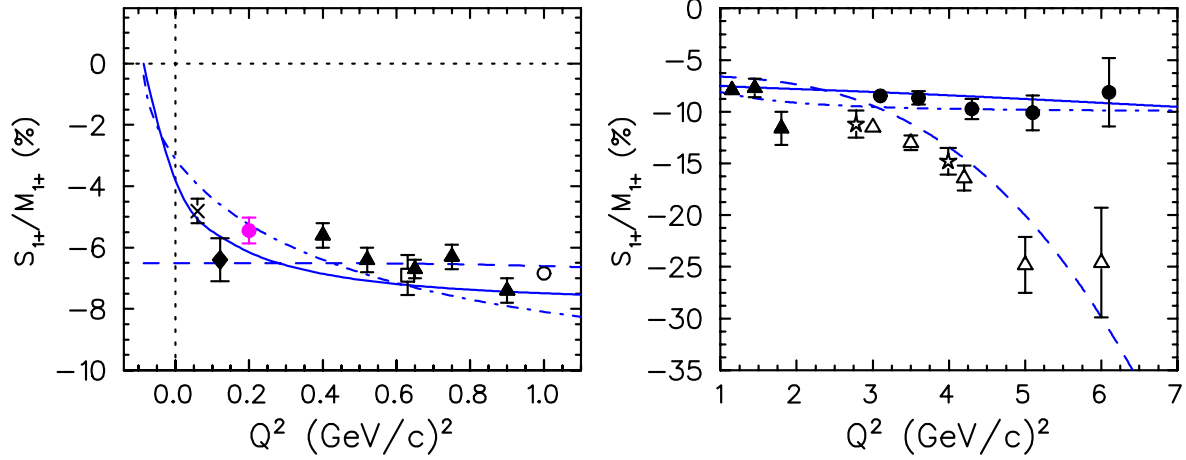


Fig. 18. The Q^2 dependence of the ratio R_{SM} at the $\Delta(1232)$ resonance position. The blue solid and dashed lines are the MAID2007 and MAID2003 super-global solutions, respectively, the dashed-dotted line is obtained using Eq. (41) with $a = 0.9$ and $d = 1.75$. The data point of Ref. [49] (diamond) at $Q^2 = 0.1$ GeV² is practically identical to the Bates result [47], the full circle at $Q^2 = 0.2$ GeV² is from Ref. [50]. See Fig. 17 for the notation of the further data points.

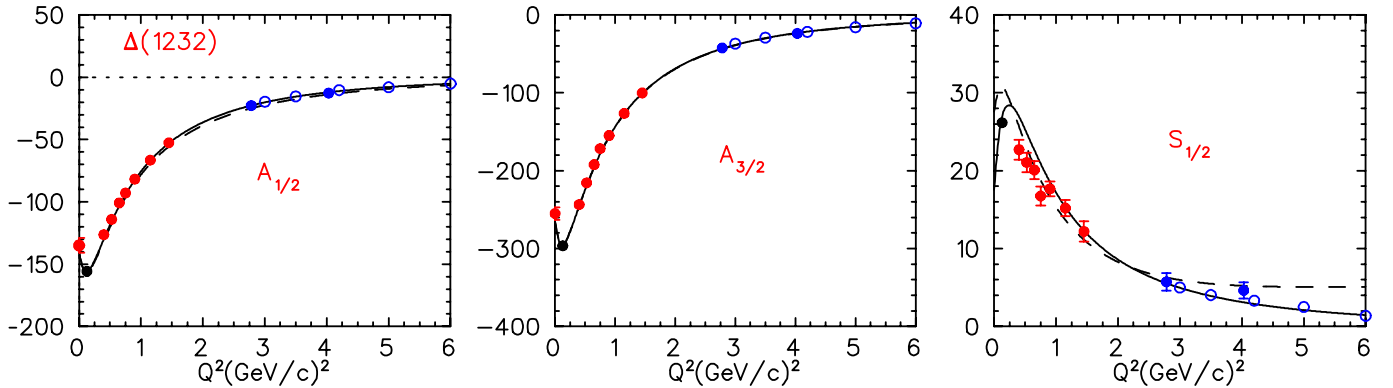


Fig. 19. The Q^2 dependence of the 3 helicity amplitudes for the $\Delta(1232)$ resonance, in units 10^{-3} GeV^{-1/2}. The solid and dashed lines are the MAID2007 and MAID2003 super-global solutions, respectively. The data points are from our single- Q^2 fits to the π^0 and π^+ CLAS data (red full and blue open circles, see Table 9 for references), Ref. [62] (blue full circles), Ref. [47] (black full circles at $Q^2 = 0.127$ GeV²), and Ref. [2] (green full circles at $Q^2 = 0$).

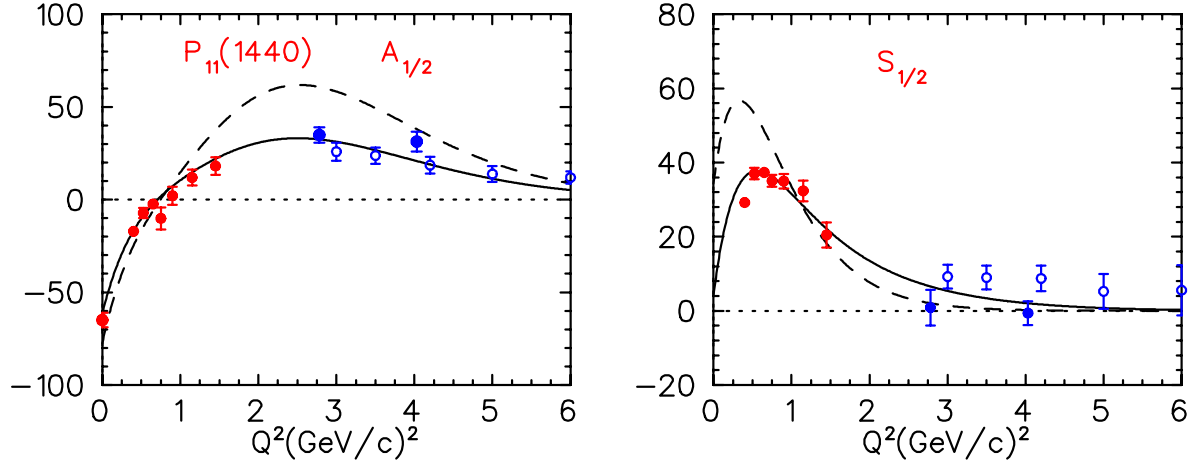


Fig. 20. The Q^2 dependence of the helicity amplitudes for the $P_{11}(1440)$ resonance of the proton. Further notation as in Fig. 19.

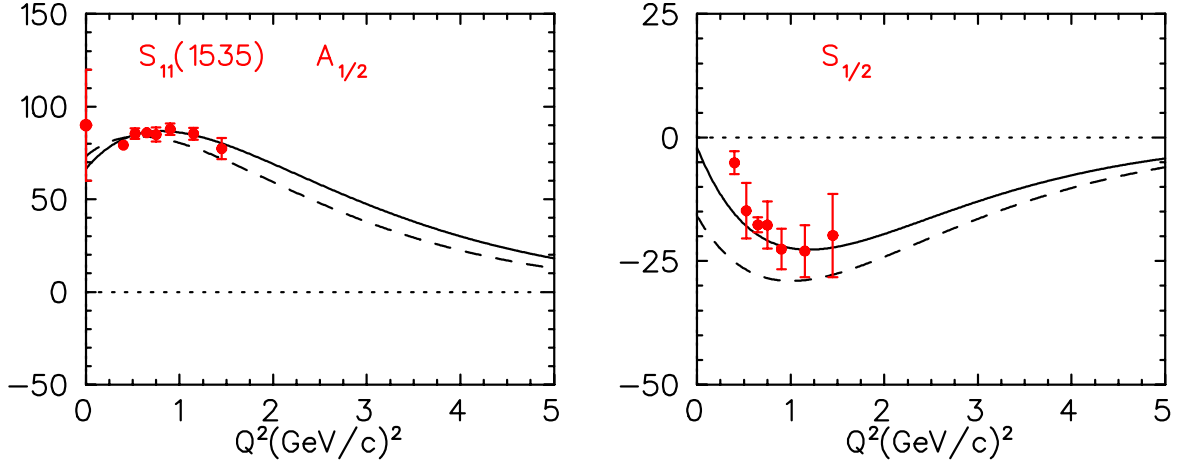


Fig. 21. The Q^2 dependence of the helicity amplitudes for the $S_{11}(1535)$ resonance of the proton. Further notation as in Fig. 19.

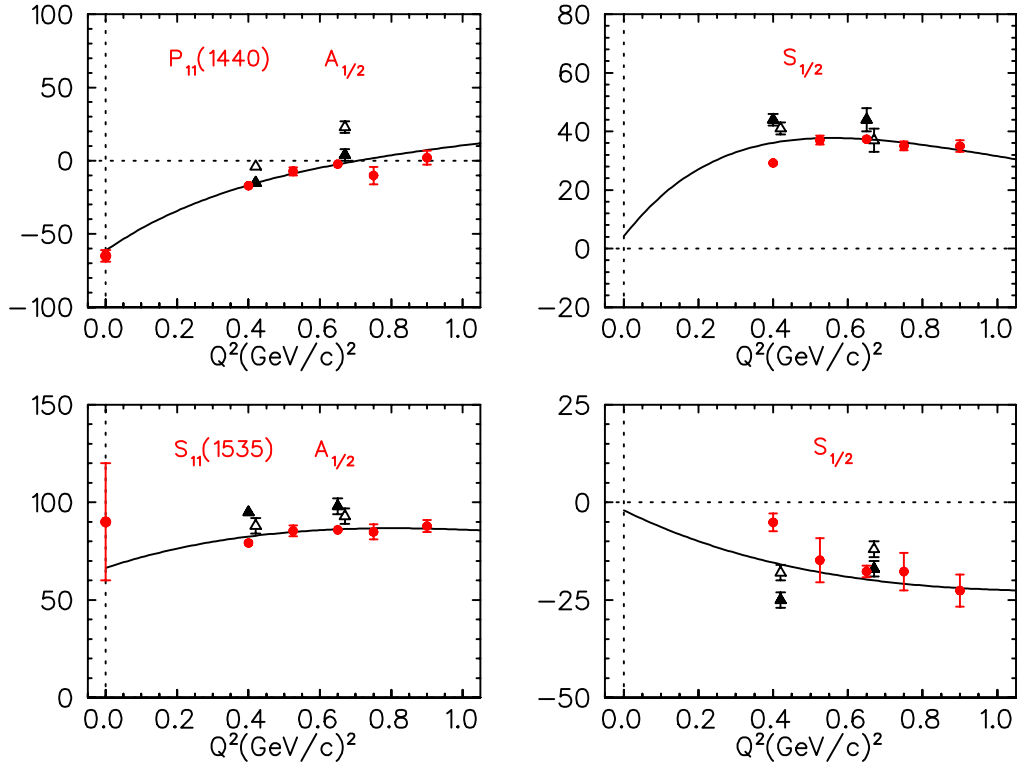


Fig. 22. The Q^2 dependence of the helicity amplitudes for the $P_{11}(1440)$ and $S_{11}(1535)$ resonances of the proton. The MAID2007 super-global analysis (solid lines) and the single- Q^2 fits (red full circles with error bars) are compared to the results of Aznauryan [64] obtained from a similar data set within an isobar model (full triangles) and dispersion theory (open triangles). Further notation as in Fig. 19.

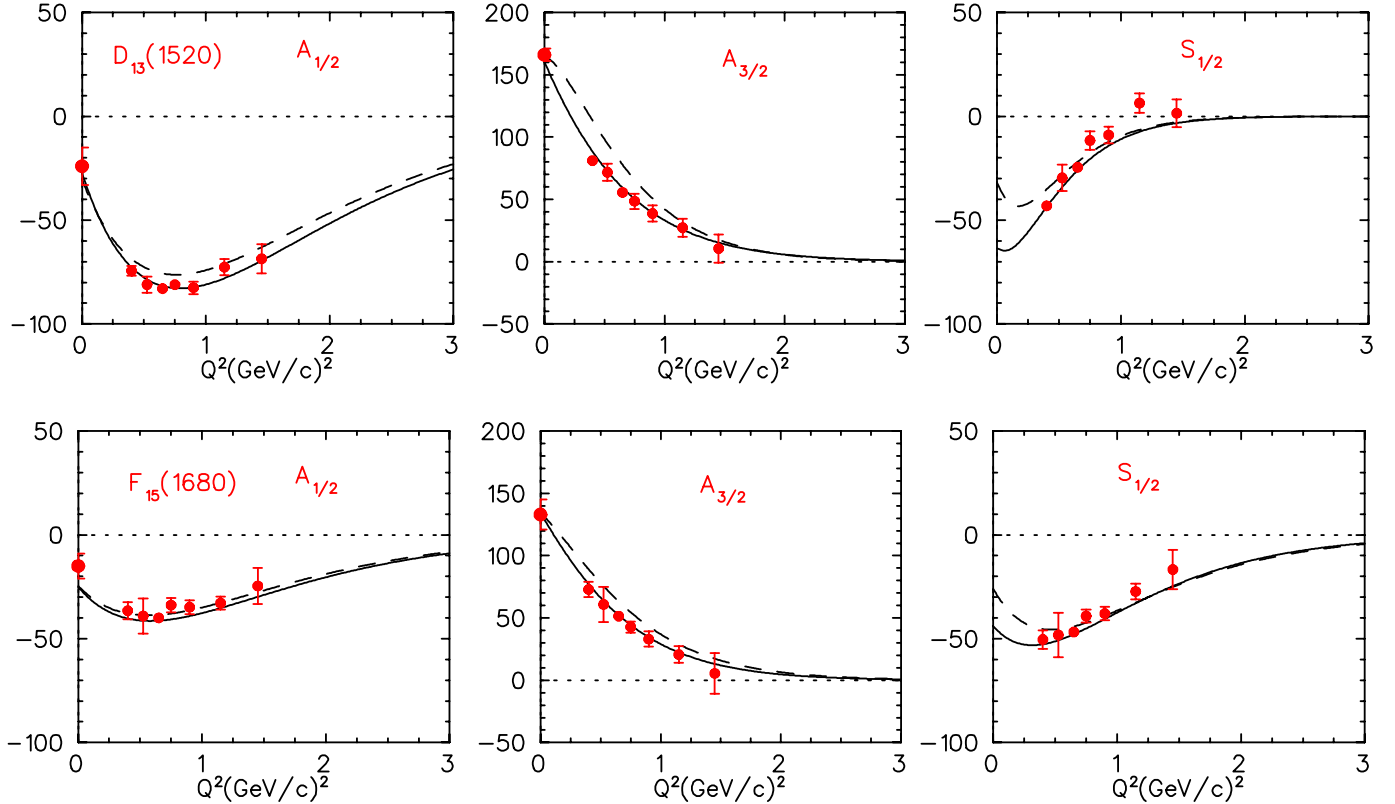


Fig. 23. The Q^2 dependence of the helicity amplitudes for the $D_{13}(1520)$ and $F_{15}(1680)$ resonances of the proton. Notation as in Fig. 19.

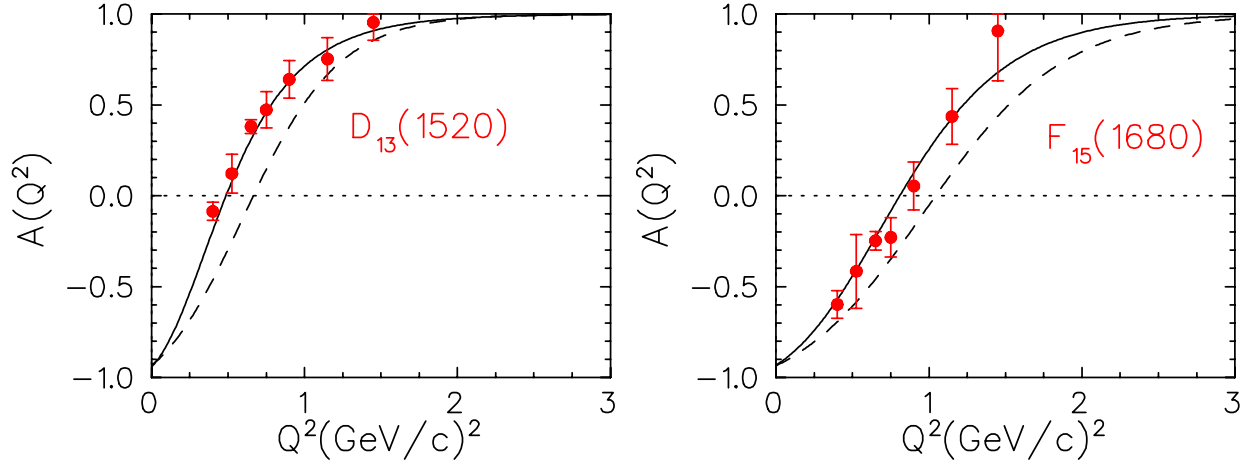


Fig. 24. The helicity asymmetry $\mathcal{A}(Q^2)$ of Eq. (48) for the $D_{13}(1520)$ and $F_{15}(1680)$ resonances of the proton. The solid and dashed curves are the super-global MAID2007 and MAID2003 solutions, respectively. The data are the results of our single- Q^2 fits to the CLAS data (red full circles, see Table 9 for references).